

Chapter 4 – Atmospheric Forcing and Remote Forcing

In order to understand physical forcing that is responsible for the basin-wide variability of mixed layer depth and barrier-layer thickness, atmospheric forcing as well as the remote forcing were examined. Towards this the atmospheric forcing such as incoming short wave radiation, net heat flux, wind speed, wind-stress curl and evaporation minus precipitation, and remote forcing such as advection of high salinity waters from the Arabian Sea and propagation of Rossby waves in the Bay of Bengal were analyzed and presented in this chapter.

4.1 Incoming short wave radiation

The incoming short wave radiation (SWR) in the Bay of Bengal during January was low and showed a spatial variation of about 25 W/m^2 within the basin, which was lowest compared with other months (Fig.4.1.1a). North of 15°N , SWR showed decreasing trend with a minimum value of 190 W/m^2 very near to the head Bay. In the central Bay SWR varied marginally between 195 and 200 W/m^2 . Highest value of SWR was seen in the Andaman Sea ($\sim 210 \text{ W/m}^2$) and west of Sri Lanka. In February SWR showed a general increase and varied from 210 W/m^2 in the head Bay to 240 W/m^2 in the southern Bay (Fig.4.1.1b). The highest SWR was in the Andaman Sea region ($\sim 250 \text{ W/m}^2$) and east of Sri Lanka (255 W/m^2) as in the case of January. The overall spatial variation in February was about 45 W/m^2 . The SWR showed a further increase in March with highest value of 280 W/m^2 occurring in the western Bay and also in the Andaman Sea (Fig.4.1.1c). The high SWR was seen within a zonal band between 8° and 18°N . Away from this region the

SWR decreased rapidly towards north as well as south with the lowest value of about 230 W/m^2 . Thus, the spatial variability of SWR in March was about 50 W/m^2 . The incoming solar radiation was the highest in the Bay in April with the highest value of 290 W/m^2 occurring in the Andaman Sea (Fig.4.1.1d). In fact the entire Bay north of 10°N was having SWR higher than 250 W/m^2 . The SWR decreased rapidly south of 15°N from 280 to 230 W/m^2 . In the head Bay SWR was about 270 W/m^2 . The spatial variation in SWR

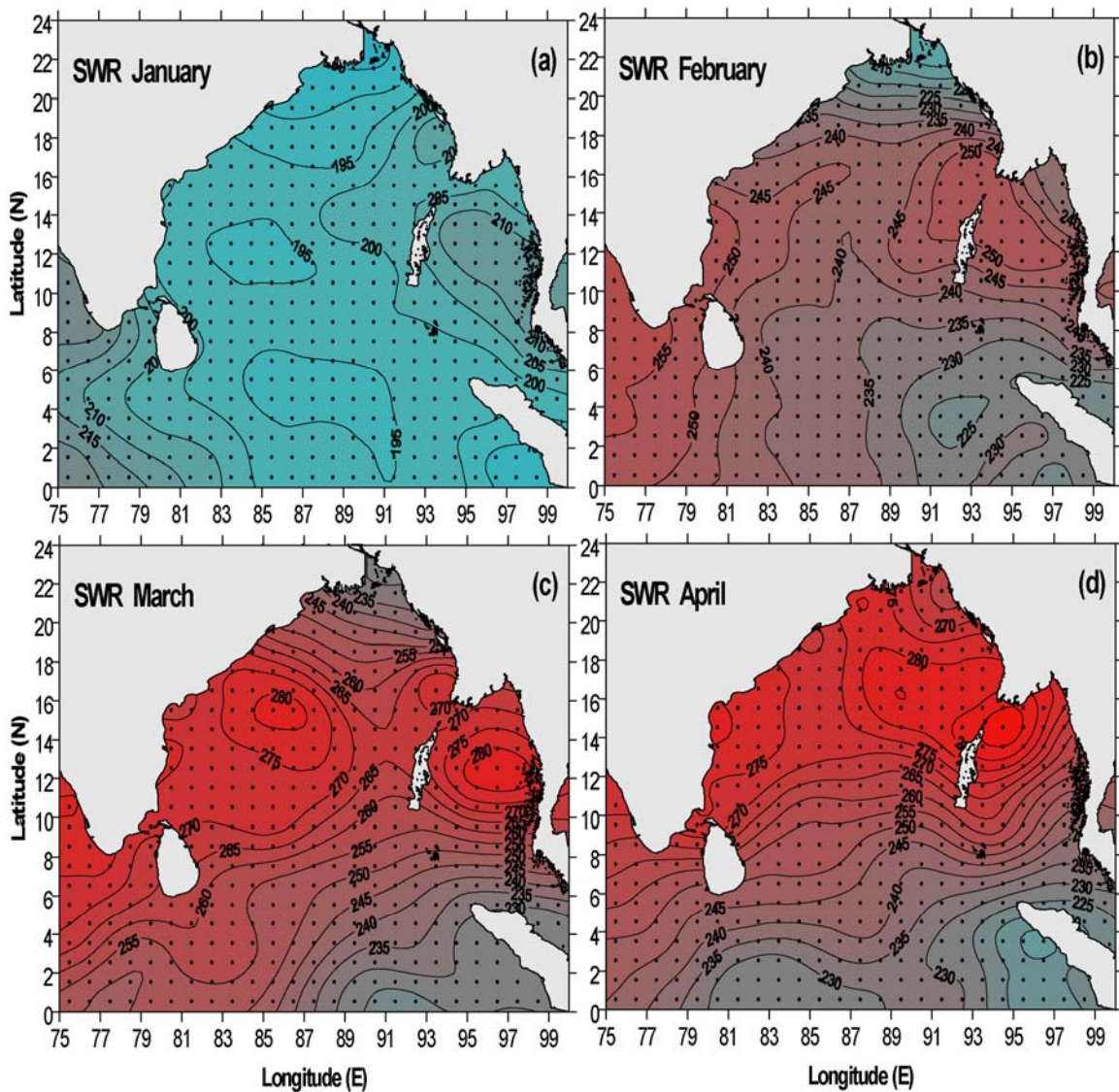


Fig.4.1.1 Monthly mean distribution of SWR (W/m^2) in the Bay of Bengal during January to April.

was about 65 W/m^2 .

During May the SWR showed a decreasing trend from north to south with highest value of 280 W/m^2 close to the northeastern boundary (Fig.4.1.2a). North of about 15°N SWR was higher than 250 W/m^2 . In the south SWR decreased rapidly and the lowest value of 195 W/m^2 was seen near the eastern equatorial region off Sumatra. The spatial variation

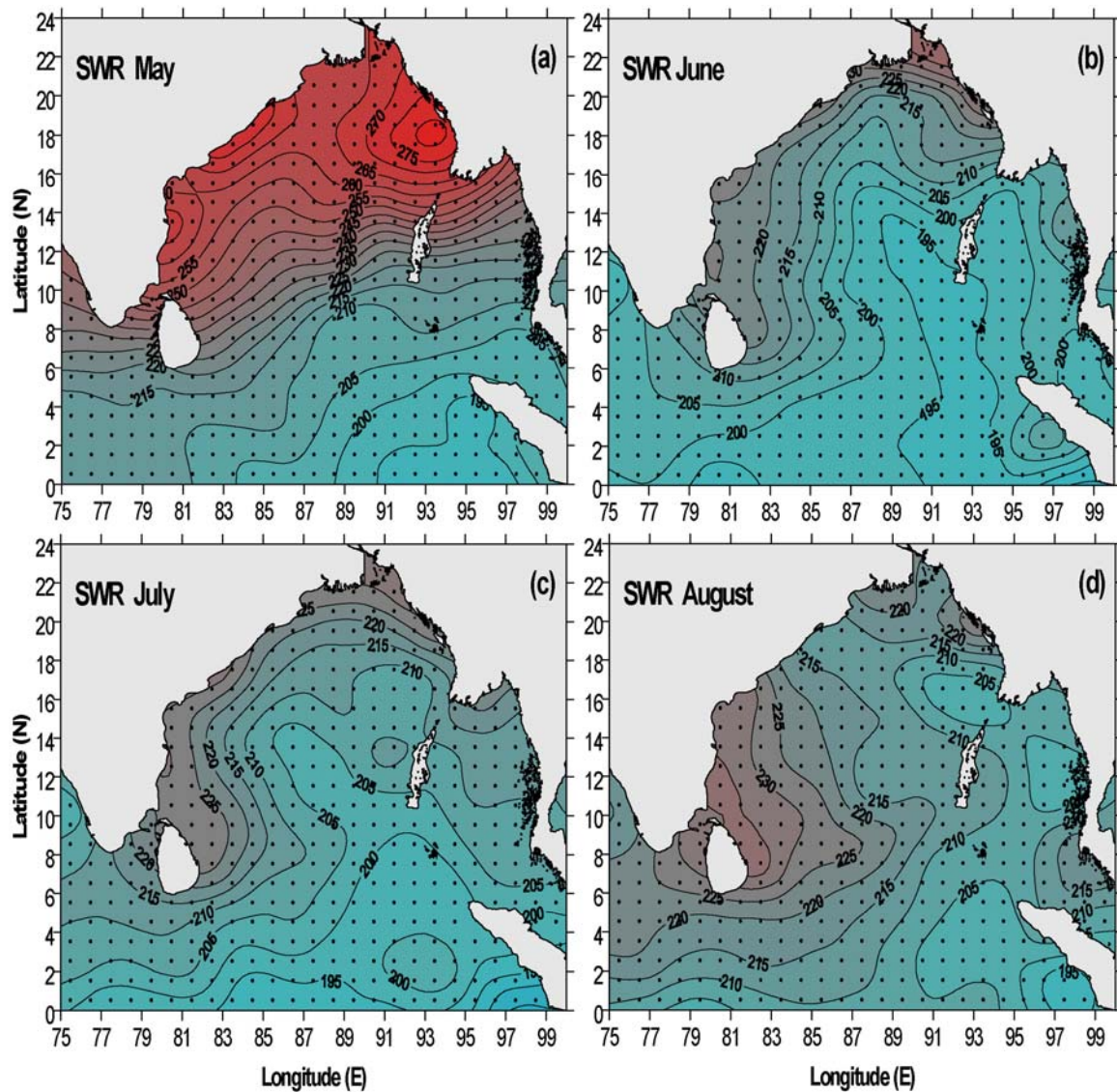


Fig.4.1.2 Monthly mean distribution of SWR (W/m^2) in the Bay of Bengal during May to August.

in SWR from south to north was about 85 W/m^2 , which was highest compared with other months. During June SWR showed a further decrease in the northern Bay with highest value of 230 W/m^2 close to the head Bay (Fig.4.1.2b). Along the western boundary SWR was about 220 W/m^2 , which decreased towards the central Bay reaching a minimum value of 195 W/m^2 . From the central Bay towards the eastern boundary the SWR showed a weak increase. The variation in the SWR from south to north was about 40 W/m^2 . In July the spatial distribution of SWR was similar to that of June except that the central and eastern Bay showed a warming of about 10 W/m^2 (Fig.4.1.2c). During August the region encompassing southern part of the western boundary and Sri Lanka showed high incoming short wave radiation with maximum value of 235 W/m^2 (Fig.4.1.2d). In the central and eastern Bay SWR were low and varied between 205 and 215 W/m^2 . The lowest SWR was 195 W/m^2 , which occurred near the Sumatra coast.

In September SWR further increased around Sri Lanka and southern part of the western boundary with maximum value of 240 W/m^2 (Fig.4.1.3a). The remaining Bay showed a distribution pattern very similar to that of August and SWR varied between 205 and 220 W/m^2 . The SWR showed least spatial variability of about 20 W/m^2 in October with highest value of 220 W/m^2 towards the west of Sri Lanka as well as close to the central part of the eastern boundary (Fig.4.1.3b). In November SWR showed a decrease, especially north of 15°N , where the value changed from 175 to 165 W/m^2 (Fig.4.1.3c). The highest value of about 230 W/m^2 occurred in the western part near the equator. In the central Bay the SWR varied between 175 W/m^2 to 195 W/m^2 . The variation in SWR from north to south was about 55 W/m^2 . A further decrease of SWR was noticed in December (Fig.4.1.3d), though the spatial distribution pattern remained similar to that of November.

The highest SWR of about 210 W/m^2 was observed very near to the equator in the western region while the lowest value of 170 W/m^2 was towards the northern Bay.

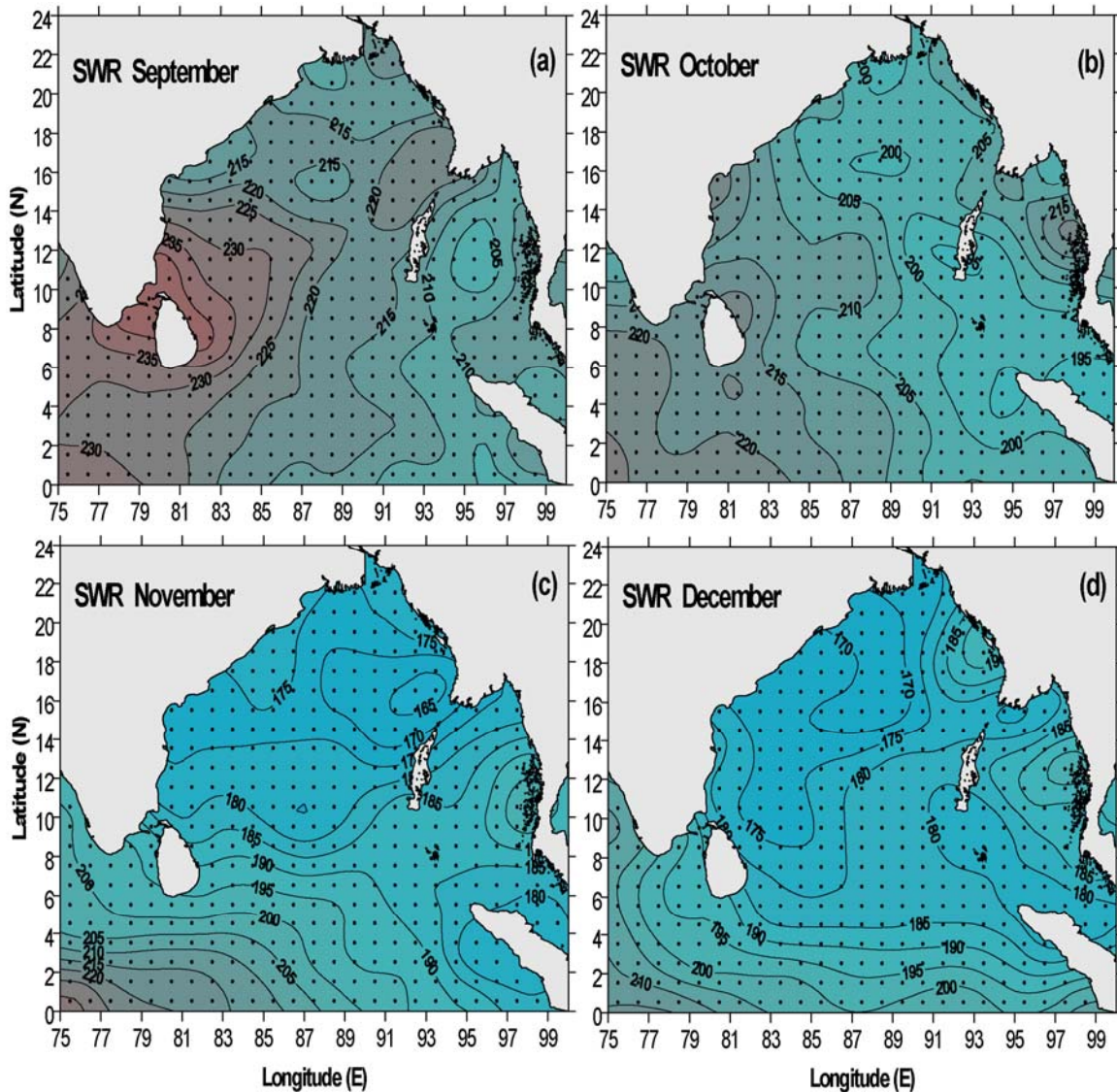


Fig.4.1.3 Monthly mean distribution of SWR (W/m^2) in the Bay of Bengal during September to December.

In summary, the amplitude of the seasonal cycle of incoming short wave radiation within the basin was about 120 W/m^2 with lowest SWR during November – December and highest during March-April. The lowest incoming short wave radiation was about 165 W/m^2 during November while highest SWR was about 285 W/m^2 , which was during

April. The seasonal cycle of SWR showed two warming period with high incoming short wave radiation during March-April and September. The period of low incoming short wave radiation was during November-February and June-August. The highest spatial variability occurred during May when SWR varied 80 W/m^2 from south to north. The least spatial variability occurred in January and October which was about 20 W/m^2 .

4.2 Net Heat Flux

Spatial distribution of the net heat flux (NHF) in the Bay of Bengal showed heat gain by the ocean in January (Fig.4.2.1a). The net heat gain was highest in the Andaman Sea, which was about 70 W/m^2 . In most part of the Bay the NHF showed very small variation, from 0 to 20 W/m^2 . Along the northern part of the western boundary NHF was 30 W/m^2 . Towards the south, south of 4°N , NHF increased to 50 W/m^2 . In February NHF showed a basin-wide increase, with highest value of 120 W/m^2 in the Andaman Sea (Fig.4.2.1b). In the northern Bay, north of 18°N , NHF showed a sharp decrease from 70 to 0 W/m^2 very near to the head Bay. The central Bay gained about 70 W/m^2 over its January value. The variation in the NHF was about 100 W/m^2 . During March entire Bay gained more heat compared to February and in the central Bay the gain was almost twice with the highest value of 150 W/m^2 (Fig.4.2.1c). The highest net heat gain in the head Bay was about 100 W/m^2 . The highest NHF was in April, which showed a spatial variation of about 90 W/m^2 (Fig.4.2.1d). The high NHF was seen as a zonal band between 11° and 13°N with highest value of 160 W/m^2 located west of 90°E . Away from this zonal band of high NHF, the values reduced towards both north and south. The lowest NHF was 70 W/m^2 and was

seen close to head Bay in the north and equator in the south. The spatial variation in net heat flux was about 90 W/m^2 .

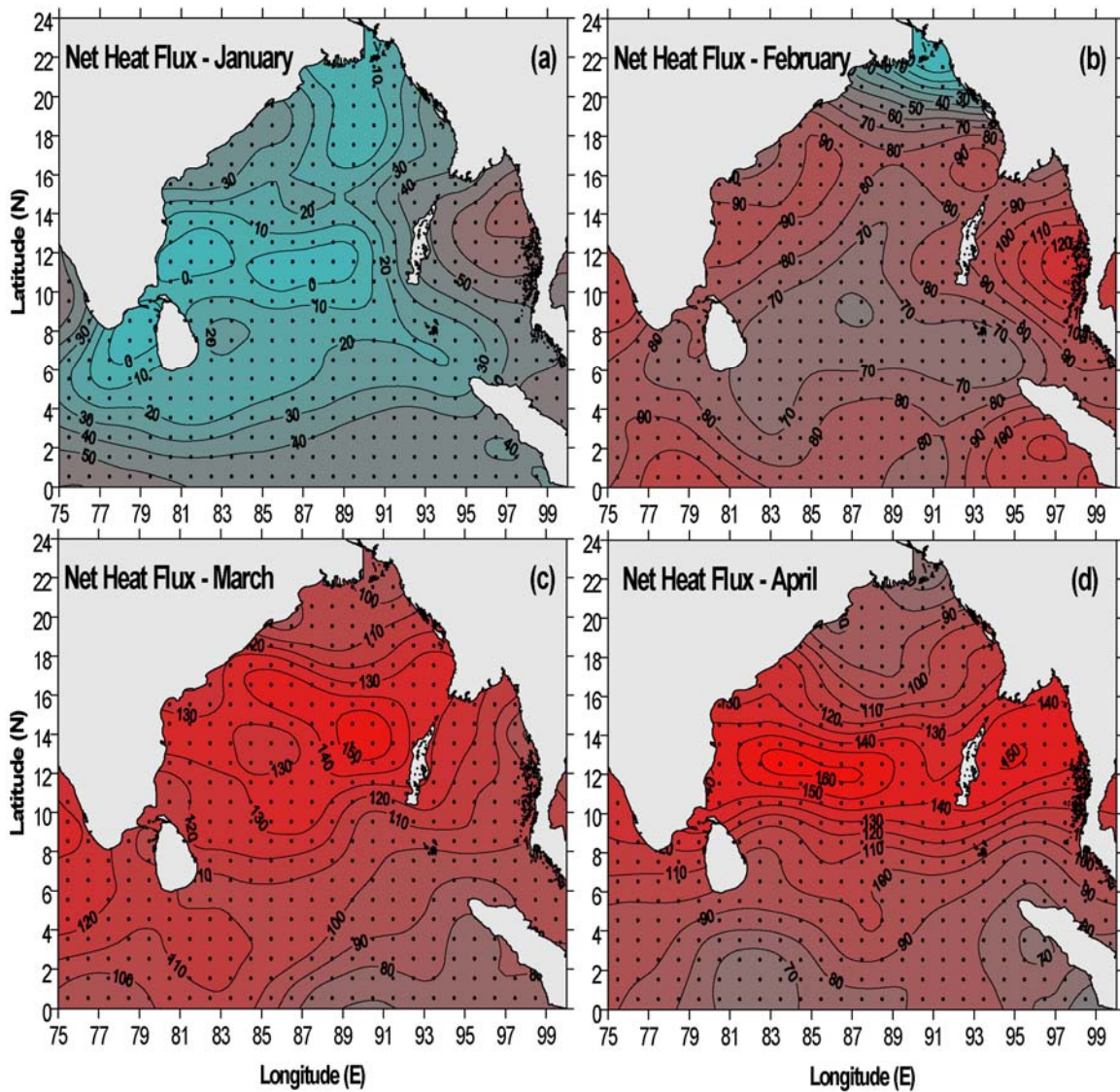


Fig.4.2.1 Monthly mean distribution of NHF (W/m^2) in the Bay of Bengal during January to April.

In May, the net heat gain showed an increase towards the western boundary with maximum value of 170 W/m^2 located near the central part of the western boundary (Fig.4.2.2a). The minimum net heat gain was in the south near equator with value of about 30 W/m^2 . The spatial variation of NHF was 140 W/m^2 .

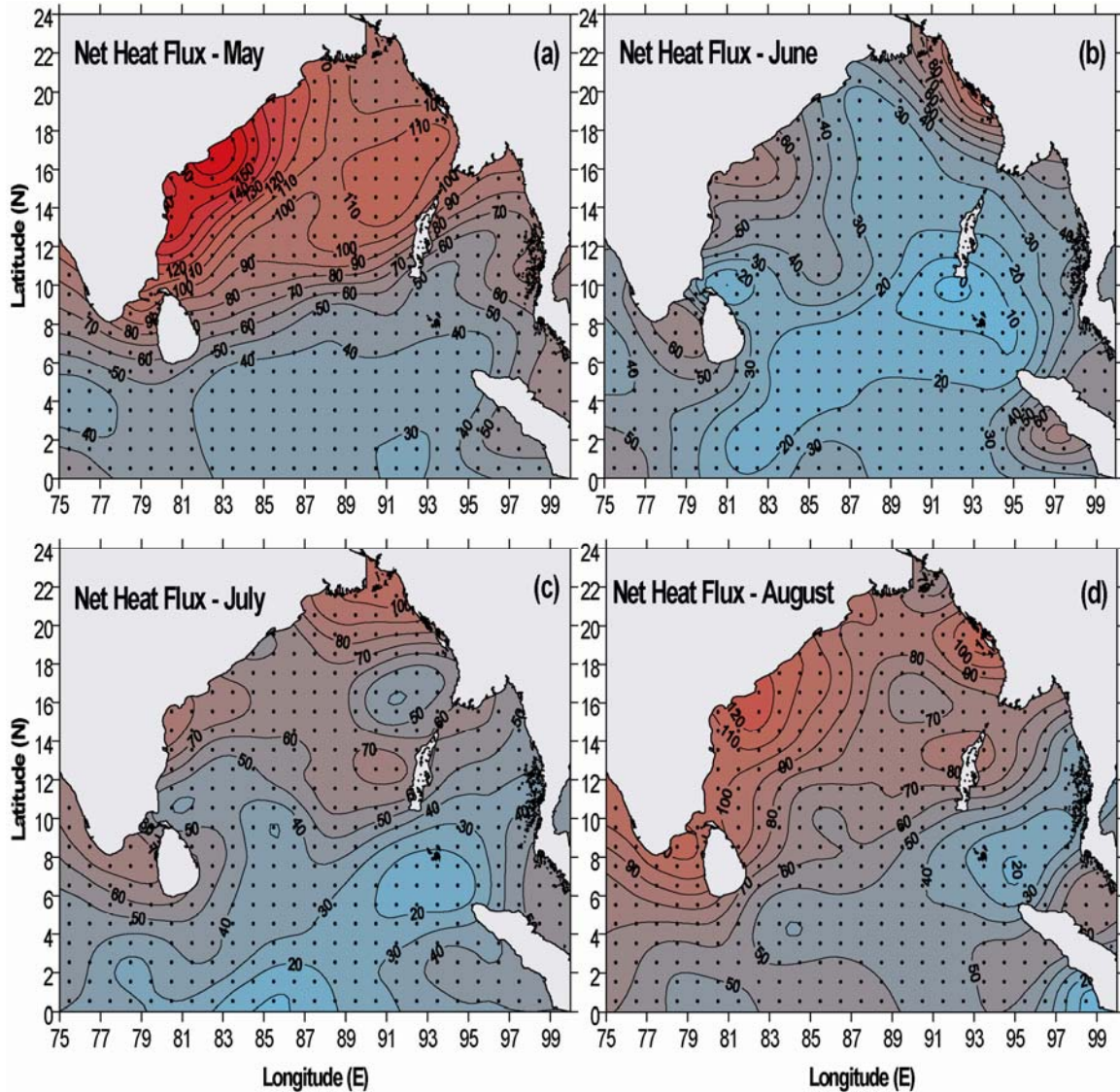


Fig.4.2.2 Monthly mean distribution of NHF (W/m^2) in the Bay of Bengal during May to August.

The NHF during June showed a basin-wide decrease with high values along the boundaries such as off peninsular India, central part of the western boundary, northeastern Bay and Sumatra coast (Fig.4.2.2b). Along the western boundary the maximum net heat gain was about 70 W/m^2 , while that along the northeastern Bay was 90 W/m^2 . The lowest NHF was observed in the southern part of the central Bay. The spatial variation in net heat flux was about 90 W/m^2 .

The spatial distribution pattern of NHF during July was similar to that of June, except that the northern Bay showed a general increase (Fig.4.2.2c). In August the entire region from the southern peninsular India, along the western boundary of the Bay, and the northeastern Bay showed high NHF (Fig.4.2.2d). In the central Bay NHF varied between 70-80 W/m^2 while the highest NHF of 120 W/m^2 occurred close to the central part of the western boundary. The lowest NHF values were seen towards south and east.

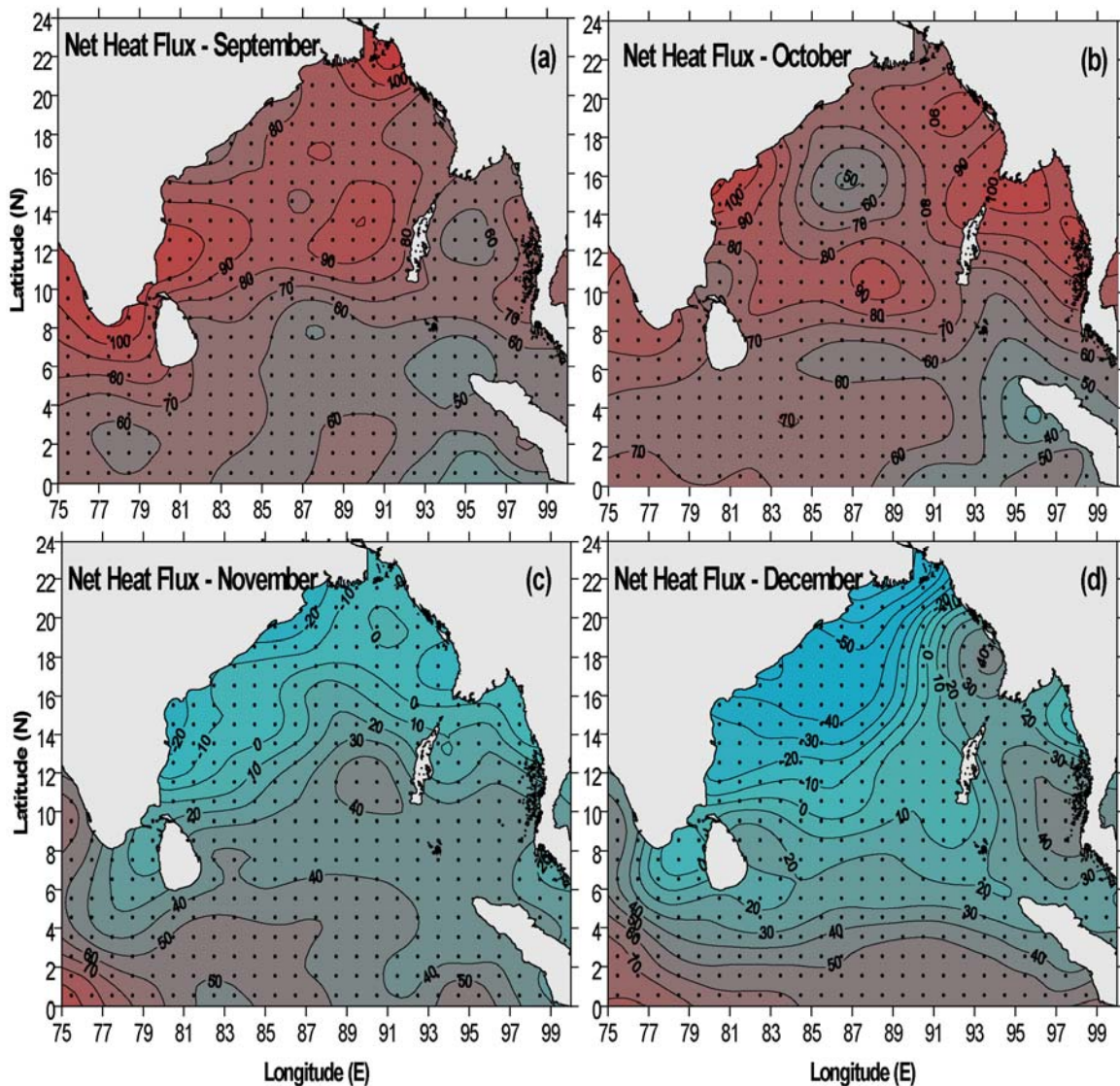


Fig.4.2.3 Monthly mean distribution of NHF (W/m^2) in the Bay of Bengal during September to December.

The NHF during September also showed the net gained by the northern Bay was higher than the southern part (Fig.4.2.3a). In the northern Bay the NHF increased from 70 to 110 W/m^2 , while in the southern part it decrease from 60 to 40 W/m^2 . The spatial variation of NHF was about 60 W/m^2 , which was lowest compared with the other months. In October a general basin-wide increase in the NHF was observed (Fig.4.2.3b). A prominent feature in the northern Bay was a region where the net heat gain was about 30 W/m^2 lower than the ambient waters. The highest NHF of 100 W/m^2 was seen close to the central part of the western as well as the eastern boundary. The lowest NHF of 40 W/m^2 was close to the Sumatra coast.

During November the NHF showed a basin-wide decrease with the northern Bay north of 15°N showing a net heat loss by about 10-20 W/m^2 (Fig.4.2.3c). Along the western boundary this loss of heat extended up to 12°N. In the southern Bay south of 10°N, the net heat gain showed an increase towards the western part and close to the equator NHF was 90 W/m^2 . In December NHF showed a further heat loss from northern Bay with a highest value of 70 W/m^2 close to the head Bay (Fig.4.2.3d). In the eastern Bay, east of 90°E and south of 20°N, NHF showed a net gain, which increased towards east with the highest value of 40 W/m^2 . South of 10°N NHF showed an increase with a maximum value of 50 W/m^2 near the equator.

In summary, the maximum net heat loss was 60 W/m^2 in the north during December and the highest net heat gain was 160 W/m^2 in the central Bay during April. The period of low Net heat flux was during December. The highest spatial variability occurred during May when Net heat flux varied by 130 W/m^2 from south to north. The least spatial

variability occurred during September, which was about 50 W/m^2 . The seasonal cycle of net heat flux in the northern Bay (north of 15°N) showed two warming period with High positive net heat flux during March-May and August-October, while low (negative) net heat flux during November-January and June. The seasonal cycle of net heat flux in the southern Bay (south of 15°N) showed semiannual variability with high net heat gain during March-April and October while low net heat during December-January and June.

4.3 Wind Speed

The spatial distribution of wind speed during January showed a zonal band of high wind speed of about 7 m/s between 6° and 12°N (Fig.4.3.1a). Within this high wind speed there were two core of highest wind speed one west of Sri Lanka with a speed of 8 m/s and the other in the central part of the Bay with a speed of 7.5 m/s . Away from this region the wind speed showed a steady decrease towards north as well as south. The lowest wind speed of 4 m/s was observed close to the head Bay as well as eastern part of the equatorial region off Sumatra. In February though the spatial pattern of wind speed distribution remained same, the strength of wind showed a decrease of about 1.5 to 2 m/s (Fig.4.3.1b). The maximum wind speed was 6 m/s and the minimum wind speed of 4 m/s was noticed close to the eastern equatorial region. The basin-wide distribution of wind speed showed the least variability in March with highest value of 5 m/s close to the northwestern boundary and the lowest value of 4 m/s in the northeastern boundary as well as in the northern part of the central Bay (Fig.4.3.1c). The wind speed showed strengthening in the northern Bay in April with highest value of 8 m/s (Fig.4.3.1d). Wind

speed decreased rapidly away from this wind speed maxima and the lowest speed of 4 m/s was noticed over a large region in southern part of the Bay.

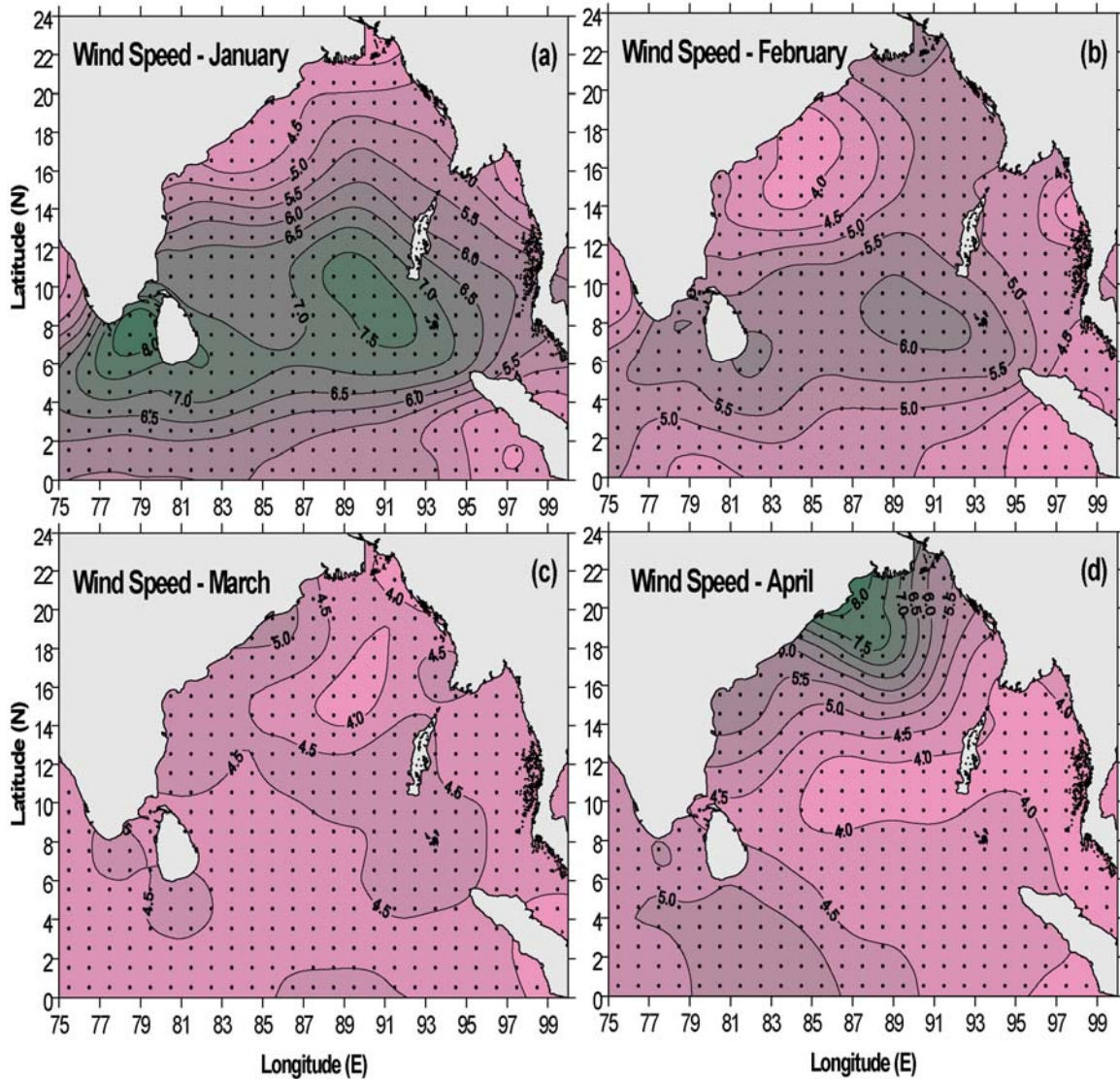


Fig.4.3.1 Monthly mean distribution of wind speed (m/s) in the Bay of Bengal during January to April.

During May two regions of high wind speed were noticed, a band along the western boundary and the other a band encompassing Sri Lanka into the central Bay in a southwest-northeast direction (Fig.4.3.2a). The highest wind speed in both the regions was 8 m/s.

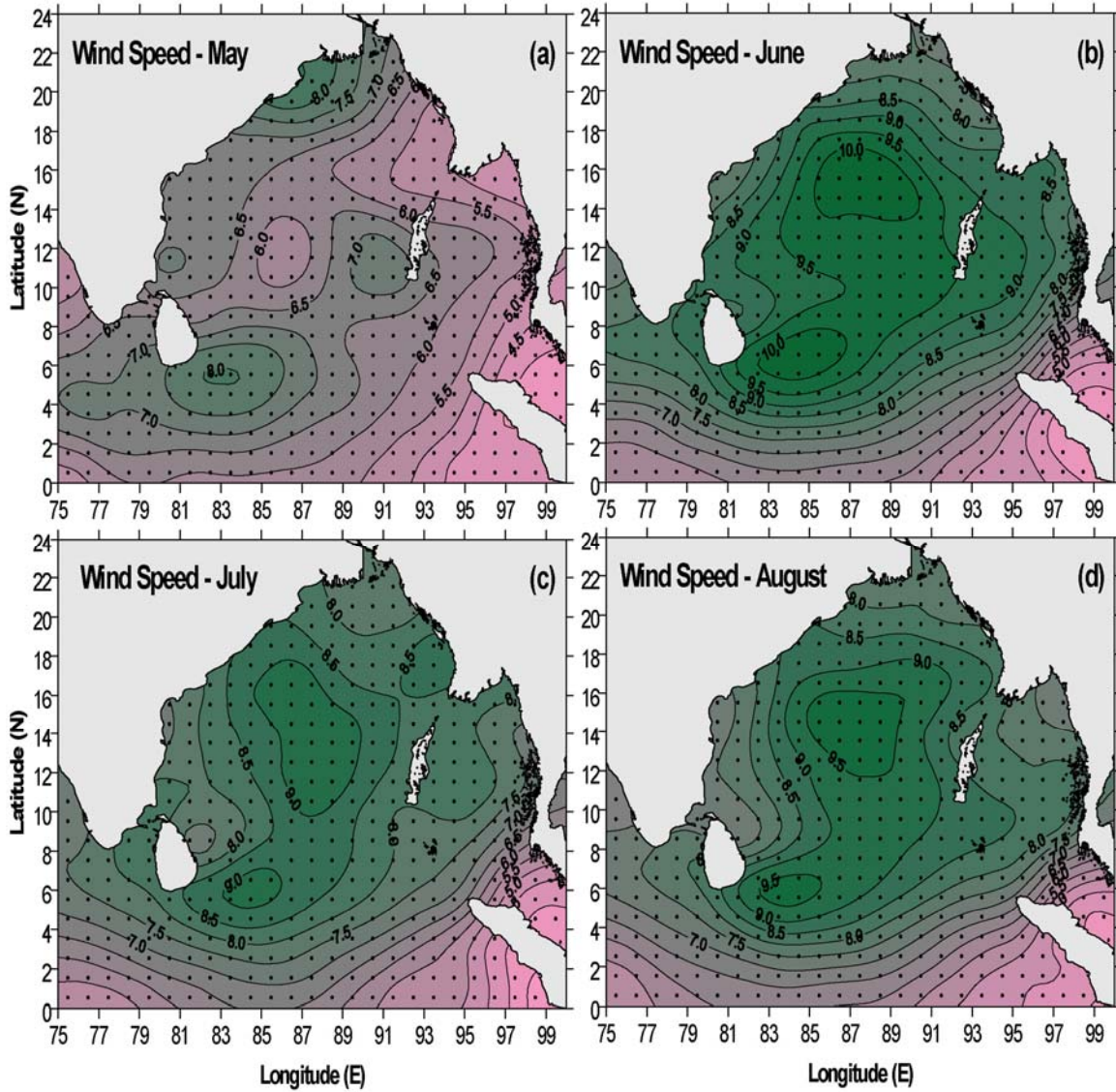


Fig.4.3.2 Monthly mean distribution of wind speed (m/s) in the Bay of Bengal during May to August.

The wind speed showed a sudden increase in June with most part of the Bay with high winds (Fig.4.3.2b). The maximum wind speed was about 10 m/s, which was the highest of all the months. In most part of the basin wind speed was between 9 and 10 m/s. The wind speed decreased towards the boundary and south of 4°N. The lowest wind speed of 6 m/s was noticed near the equator. Another region of low wind speed was observed near the southeastern Bay with minimum value of 4 m/s. Both during July (Fig.4.3.2c) and

August (Fig.4.3.2d) the spatial distribution pattern of wind remained similar. However, during July the highest wind speed in the central Bay showed a reduction of 1 m/s compared to June. In contrast, during August the speed increased by 0.5 m/s in the central Bay compared to July.

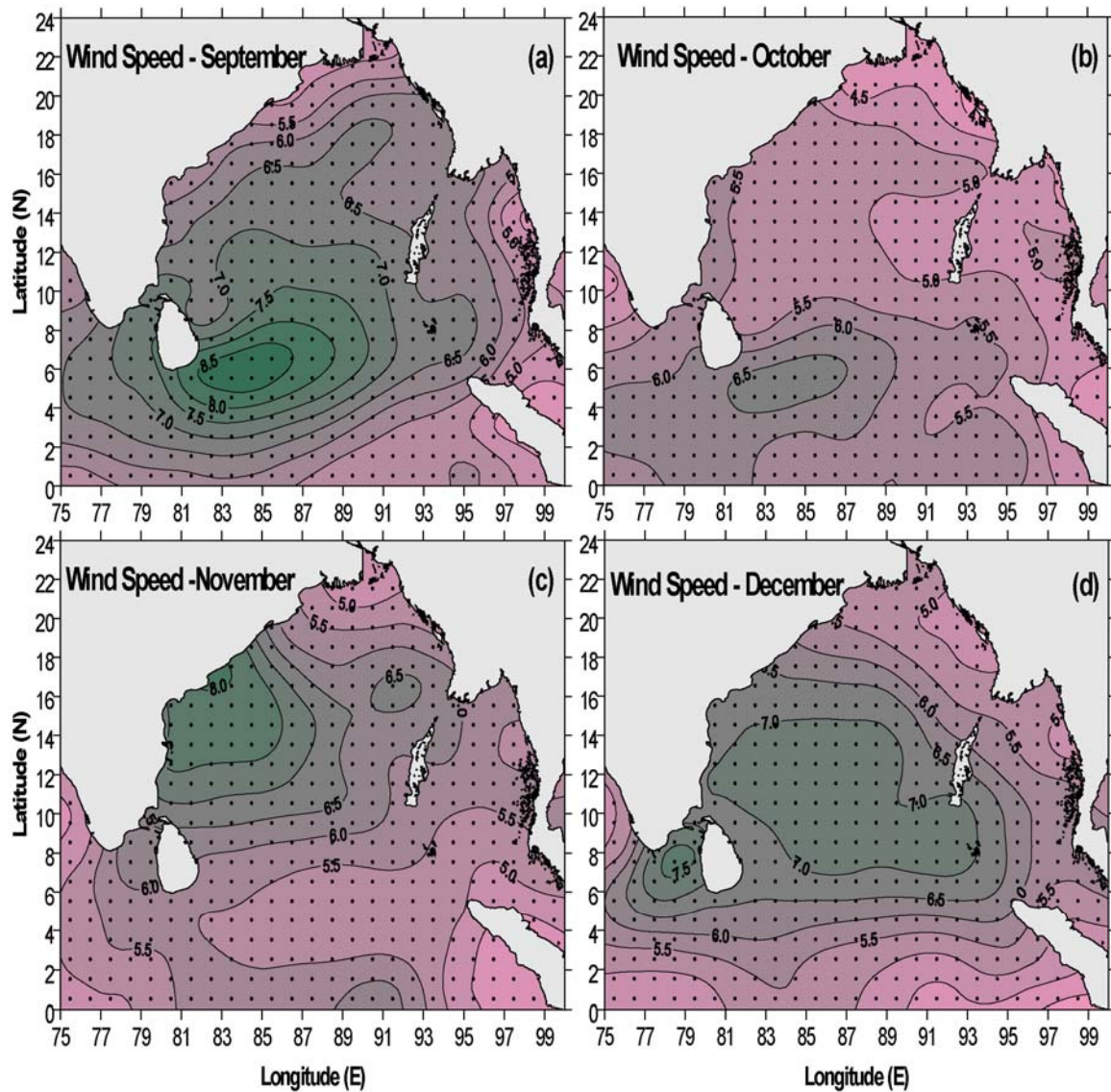


Fig.4.3.3 Monthly mean distribution of wind speed (m/s) in the Bay of Bengal during September to December.

During September the wind speed over the Bay decreased and the core of the high wind speed was located in a southwest-northeast direction off Sri Lanka (Fig.4.3.3a). The

highest wind speed was 8.5 m/s and the speed showed a steady decrease towards the north with lowest value of 4 m/s close to the head Bay. The wind speed further reduced in October and the core of the high wind speed was located in a small region south of Sri Lanka (Fig.4.3.3b). The highest wind speed was 6.5 m/s, while the lowest value was 4.5 m/s in the northern Bay. The spatial variation of the wind speed was about 2 m/s. In November a region of high wind speed of 8 m/s was noticed in the central part of the western boundary (Fig.4.3.3c). Away from the western boundary the wind speed decreased rapidly towards north as well as south. In the head Bay the lowest wind speed was 5 m/s, while in the eastern part of the equator it was 4.5 m/s. During December the region of high wind speed expanded into the central Bay, but the strength reduced to 7 m/s. Again towards north and south of this high wind speed band the value decreased.

In summary, the amplitude of the seasonal cycle of wind speed within the basin was about 6 m/s with lowest wind speed of about 4 m/s and highest wind speed of about 10 m/s. The highest wind speed occurred during June while lowest wind speed occurred during February-April. The highest spatial variability occurred during June when wind speed varied by 6 m/s from south to north. The least spatial variability occurred during March, which was about 1 m/s. The seasonal cycle of wind speed in the northern Bay (north of 15°N) showed semiannual cycle with high wind speed during June-August and November-December, while low wind speed was during January-March and October. The seasonal cycle of wind speed in the southern Bay (south of 15°N) showed semiannual variability with high wind speed during June-August and January while low wind speed during March-April and October-November.

4.4 Wind stress curl

The wind-stress curl during January showed negative curl in the northern Bay, north of 12°N, while towards the south the curl was positive (Fig.4.4.1a). The negative curl showed an increase towards the north. The highest positive curl was noticed in the southeastern region. The negative wind stress curl in the north would lead to downward

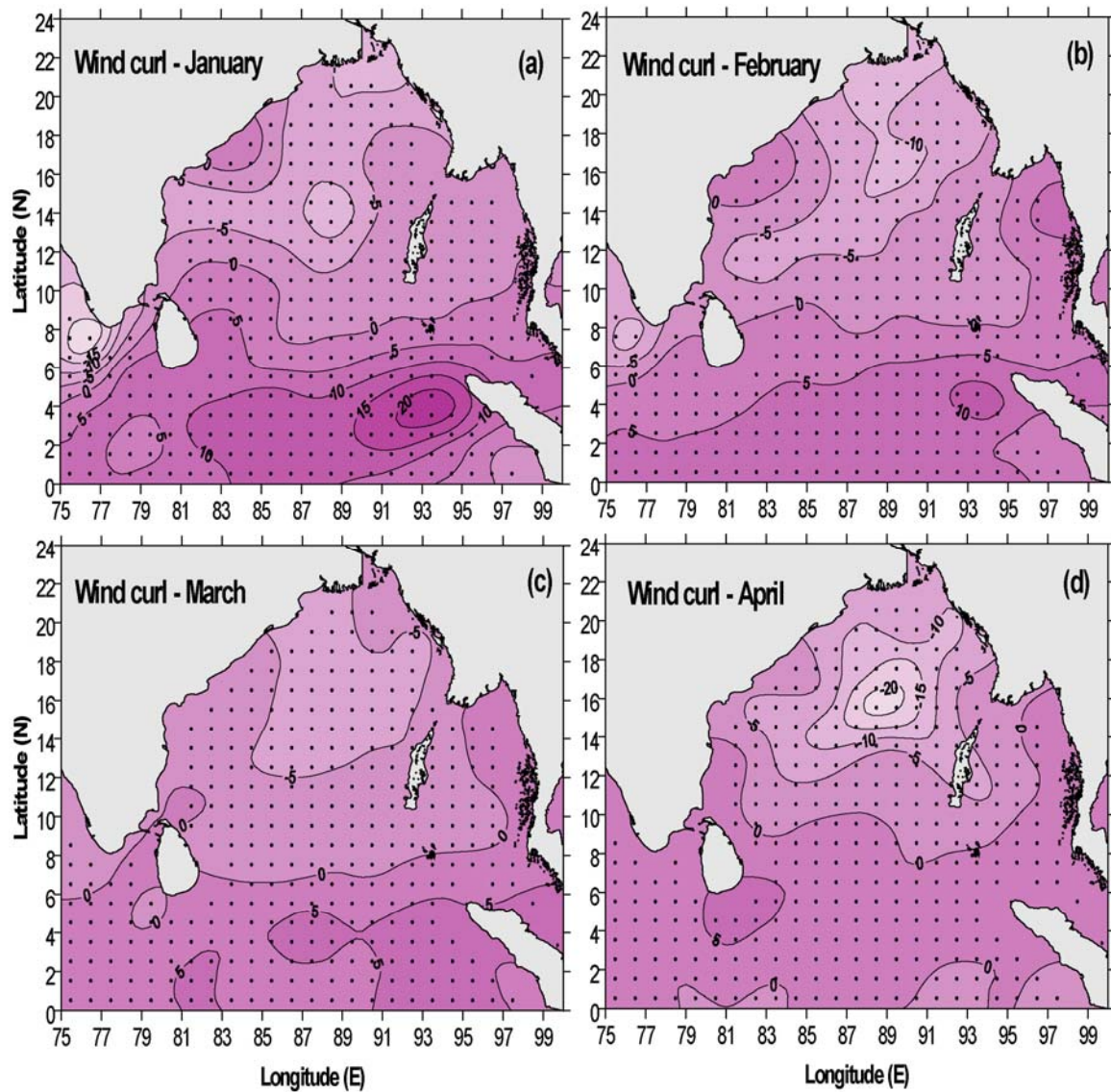


Fig.4.4.1 Monthly mean distribution of wind stress curl ($\times 10^{-8}$ Pascal/m) in the Bay of Bengal during January to April.

Ekman pumping and downwelling, while the positive curl would lead to upward Ekman pumping and upwelling. The region around southern tip of Indian Peninsula also showed a negative wind stress curl. In February the wind stress curl showed a weakening in the south, south of 12°N , and mild strengthening in the northern Bay (Fig.4.4.1b). The region of negative wind stress curl expanded further south in March but its strength in the northern Bay weakened slightly (Fig.4.4.1c). In April the region north of 8°N showed negative wind stress curl and a very strong curl region was noticed with its core located between 14° and 18°N (Fig.4.4.1d). This indicated strong downward Ekman pumping and downwelling.

During May the spatial distribution of the wind stress curl showed two regions of negative values, one a band oriented parallel to the western boundary encompassing the head Bay and part of northeastern Bay, and the other south of 4°N (Fig.4.4.2a). A strong positive wind stress curl was noticed in the region encompassing the tip of peninsular India. The positive wind stress curl would drive an upward Ekman pumping and upwelling. In the north the negative wind stress curl would lead to downward Ekman pumping. In June the entire Bay approximately north of 5°N , except towards the southeastern region, showed positive wind stress curl (Fig.4.4.2b). The region of strong positive curl east of Sri Lanka and along the western boundary would lead to strong upward Ekman pumping. South of 5°N the wind stress curl was negative. In July the distribution pattern remained the same as that of June, except an intensification of positive wind stress curl seen close to the northeastern Bay (Fig.4.4.2c). During August, the positive wind stress curl east of Sri Lanka intensified much more than June indicating stronger upward Ekman pumping (Fig.4.4.2d). The region of positive wind stress curl

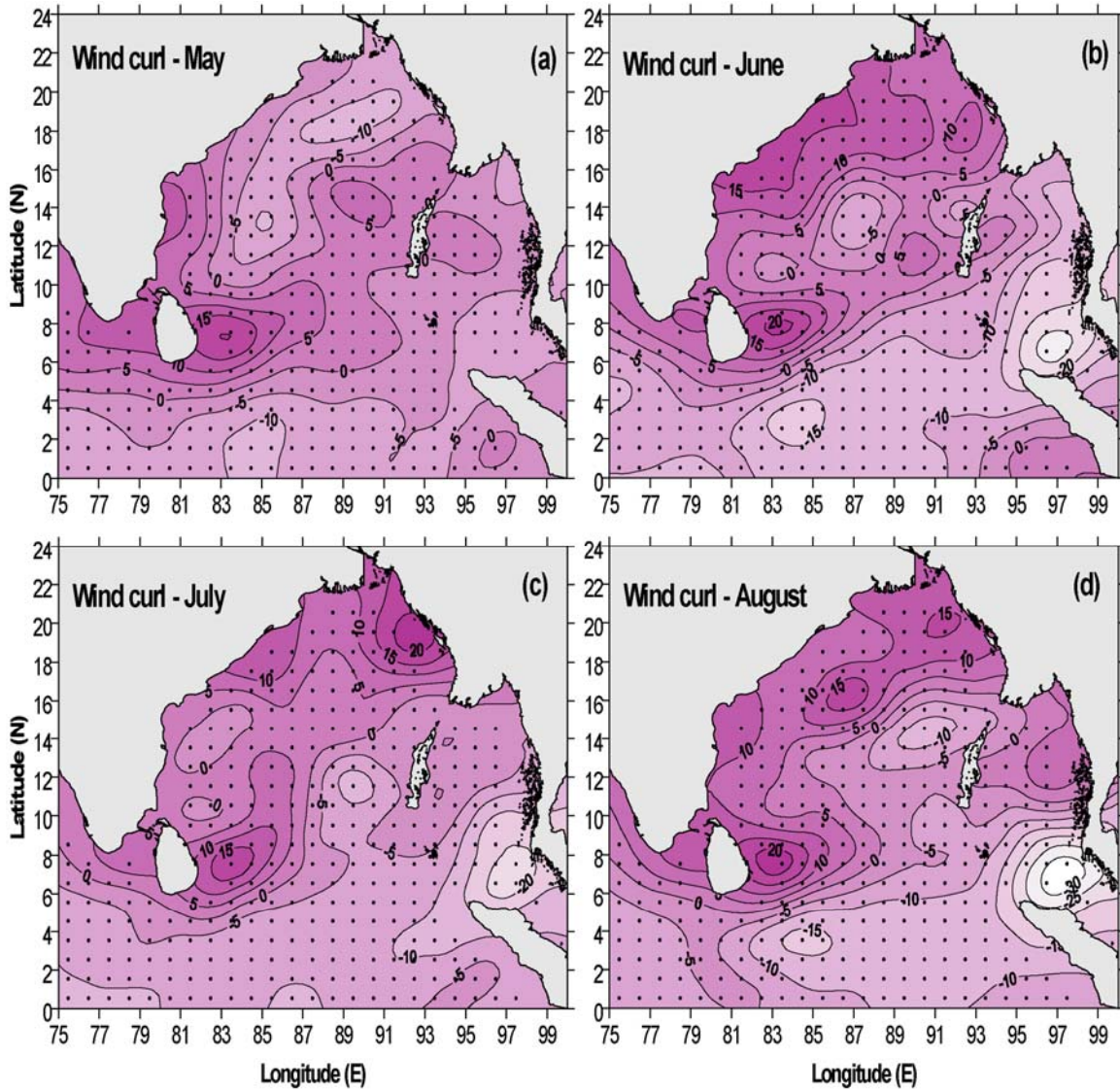


Fig.4.4.2 Monthly mean distribution of wind stress curl ($\times 10^{-8}$ Pascal/m) in the Bay of Bengal during May to August.

seen off the northeastern boundary in June extends further offshore in the southwest direction making the entire western boundary a region of upward Ekman pumping.

In September there was a general reduction in the value of wind stress curl both positive as well as negative (Fig.4.4.3a). The wind stress curl showed further reduction in October when the values over the Bay was the least (Fig.4.4.3b). In November the wind stress curl

showed an increase and almost the entire Bay showed positive values (Fig.4.4.3c). In addition, these positive wind stress curl showed a strengthening towards the western boundary. During December the wind stress curl once again showed a weakening in the northern Bay and the values were negative, while the southern Bay showed a strengthening of positive wind stress curl.

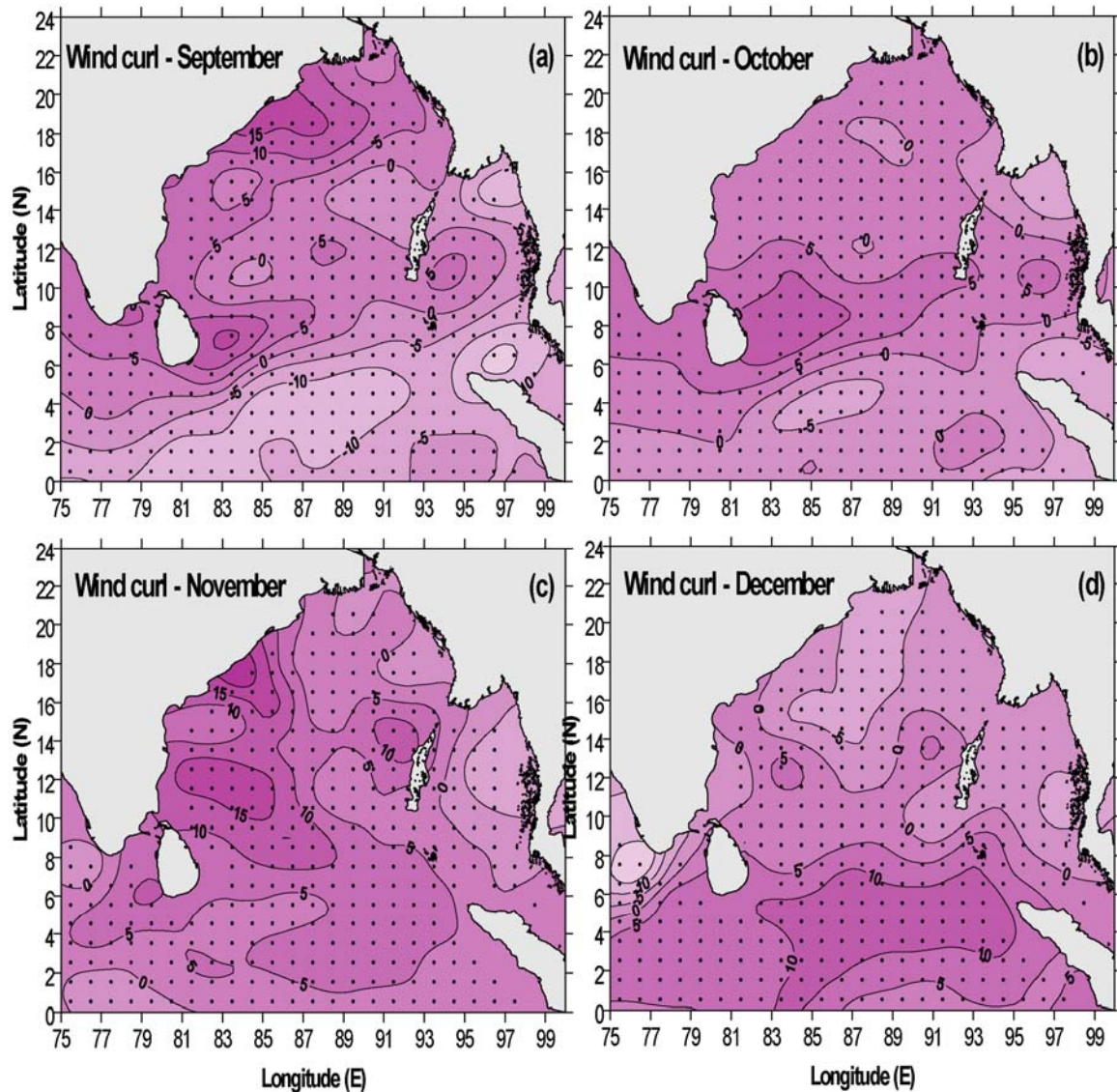


Fig.4.4.3 Monthly mean distribution of wind stress curl ($\times 10^{-8}$ Pascal/m) in the Bay of Bengal during September to December.

In summary, the maximum negative wind stress curl was about 30×10^{-8} Pascal/m which occurred during August along the southeastern boundary of Bay of Bengal while highest positive wind stress curl was about 20×10^{-8} Pascal/m which occurred during January along the south eastern Bay and also during June to August along the eastern part of Sri Lanka. The highest spatial variability occurred during August when wind stress curl varied from -30 to 20×10^{-8} Pascal/m. The least spatial variability occurred during March, when wind stress curl varied between -5 to 5×10^{-8} Pascal/m. The seasonal cycle of wind stress curl in the northern Bay (north of 15°N) showed annual cycle with positive wind stress curl from June-November and negative during December-May. The seasonal cycle of wind stress curl in the southern Bay (south of 15°N) showed annual variability with positive wind stress curl from November-March and negative wind stress curl from June-September.

4.5 Evaporation – Precipitation

The spatial distribution of evaporation minus precipitation (E-P) in January showed a net evaporation in the region north of 8°N , while south of it, there was a net precipitation (Fig.4.5.1a). The maximum evaporation of 120 mm/month was observed in the northeastern region and the maximum net precipitation of 240 mm/month was near equator. In February most part of the Bay showed net evaporation, though the magnitude of it was lower than the previous month by about 20 mm/month (Fig.4.5.1b). The region of net precipitation shifted to south of 4°N and the maximum value was 80 mm/month. During March the entire Bay showed a net evaporation of about 70-80 mm/month (Fig.4.5.1c). The region near the eastern part of the equator was the only place where E-P

showed a net precipitation with a maximum value of 80 mm/month. The spatial distribution of E-P showed a change in April with the highest net evaporation shifting from head Bay to the central part of the western boundary, which was 80 mm/month (Fig.4.5.1d). The head Bay showed a decreasing net evaporation from 40 to 10 mm/month. South of 4°N E-P showed net precipitation with the maximum value of 110 mm/month close to Sumatra coast.

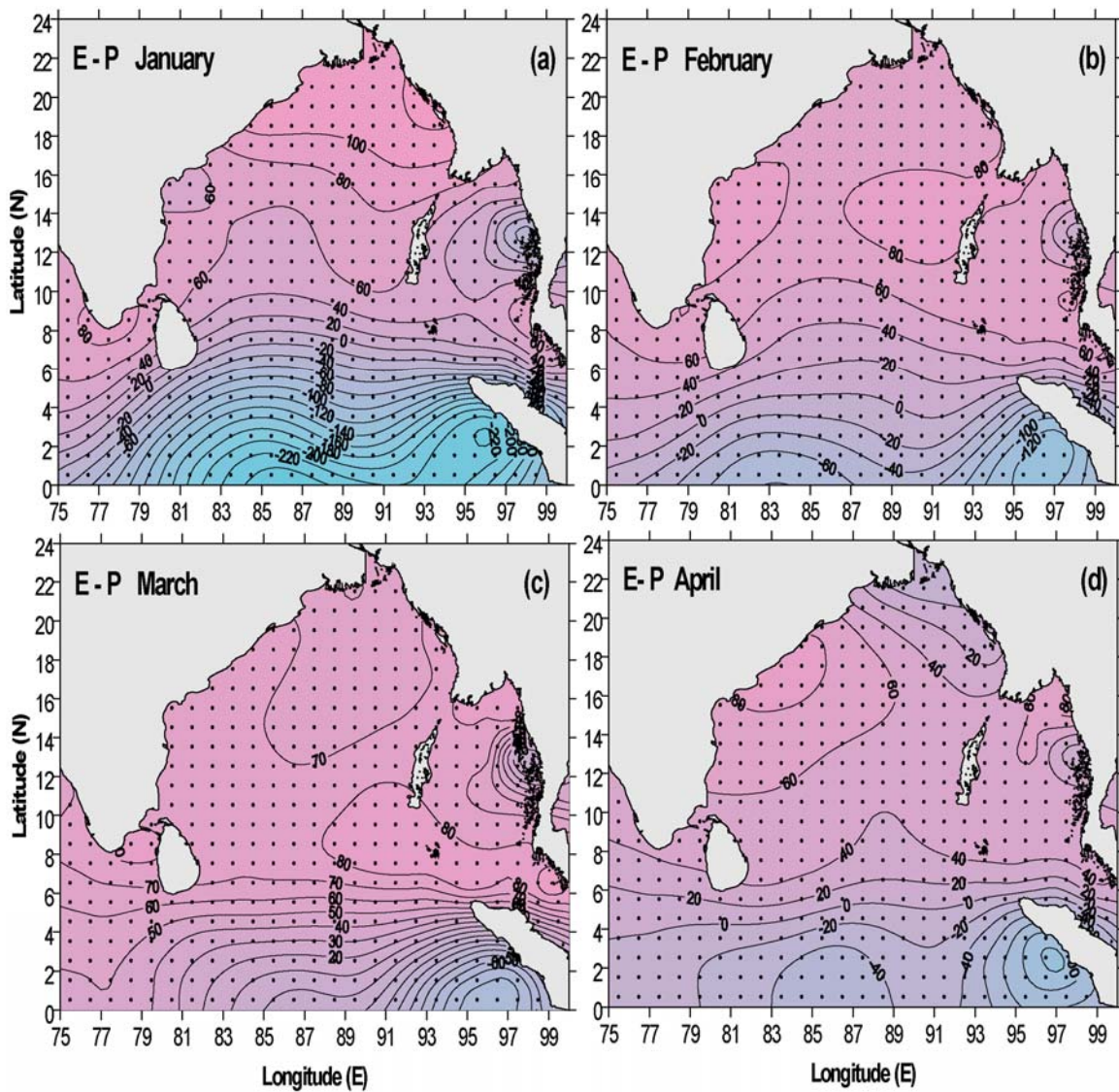


Fig.4.5.1 Monthly mean distribution of E-P (mm/month) in the Bay of Bengal during January to April.

In May the head Bay showed a net precipitation of about 80 mm/month in addition to a region in the southeastern part of the Bay with a value of 20 mm/month (Fig.4.5.2a). The rest of the Bay showed a net evaporation increasing towards west with the highest value of 80 mm/month around Sri Lanka. The E-P showed a dramatic change in its distribution pattern in June with a net precipitation in the entire Bay of Bengal except in region close to Sri Lanka, which showed a net evaporation (Fig.4.5.2b). The huge net precipitation

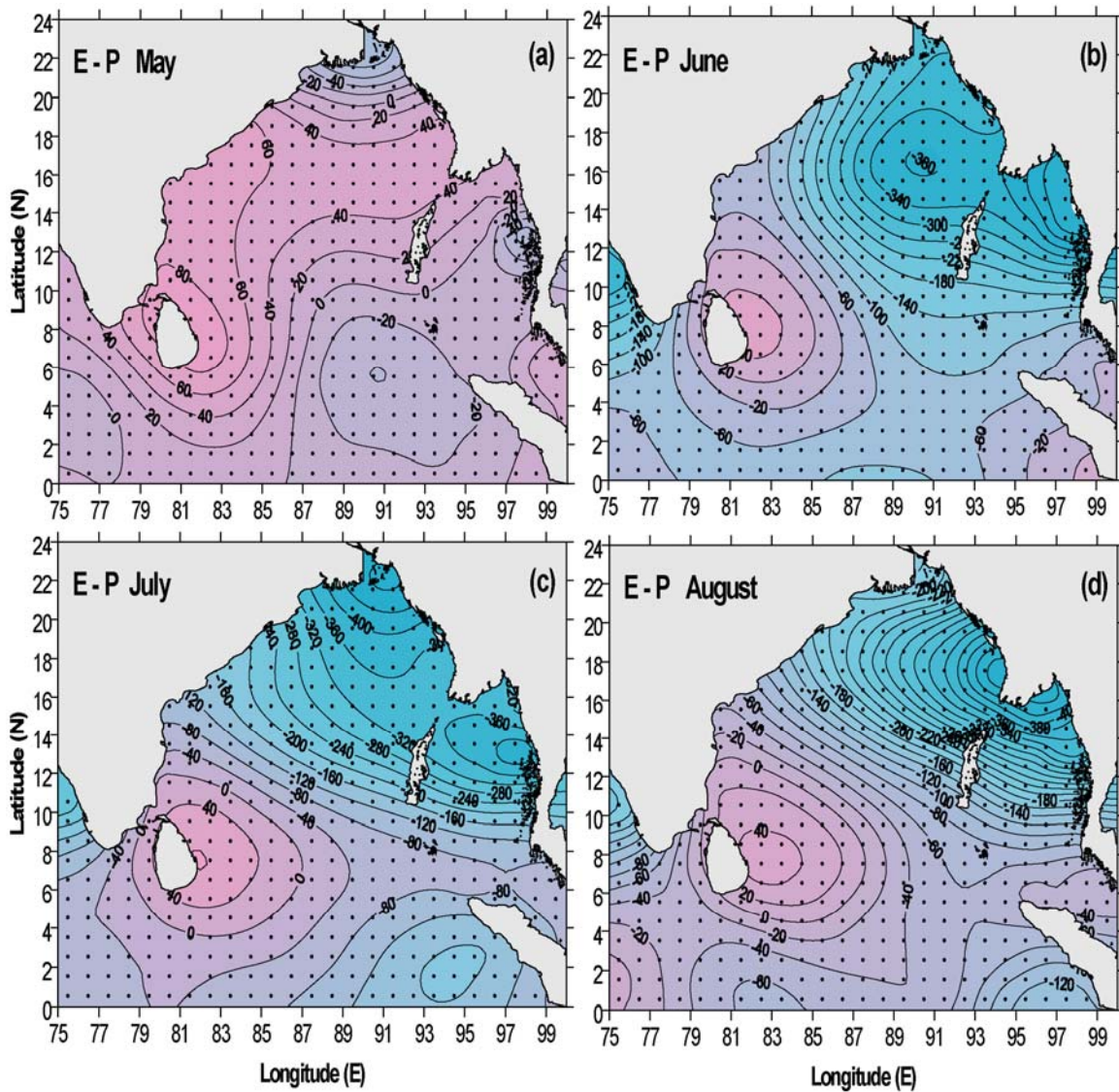


Fig.4.5.2 Monthly mean distribution of E-P (mm/month) in the Bay of Bengal during May to August.

was concentrated in a region encompassing the northwestern Bay, central Bay and the eastern boundary with the maximum value of 380 mm/month. The peninsular India showed a maximum net precipitation of 260 mm/month. The highest net evaporation around Sri Lanka was 60 mm/month. In July the pattern of E-P distribution remained similar, but the values showed an increase (Fig.4.5.2c). The highest net precipitation was 480 mm/month and was in the head Bay. The highest net evaporation around Sri Lanka showed a reduction and was 40 mm/month. During August also, the distribution pattern was similar to that of July but the net precipitation showed the maximum value of 440 mm/month in the northeastern Bay (Fig.4.5.2d). This was the highest net precipitation compared to all the months. Near the Indian Peninsula the highest net precipitation was 180 mm/month.

During September the entire Bay showed net precipitation except the region north of Sri Lanka but the values reduced drastically (Fig.4.5.3a). The highest precipitation in the northern Bay was 220 mm/month while that in the southeastern region was 280 mm/month. In October the E-P showed further reduction in their values with the entire Bay showing a net precipitation (Fig.4.5.3b). The highest net precipitation in the northern Bay was 140 mm/month near the northeastern boundary, while in the southern region it was about 220 mm/month. The region of net evaporation around Sri Lanka in September changed to net precipitation. In November, the region close to central part of both western and eastern boundary showed net evaporation while the rest of the Bay showed net precipitation (Fig.4.5.3c). The maximum precipitation was near southern Bay, which was about 180 mm/month while the maximum evaporation was about 60 mm/month. During December E-P showed net evaporation north of 12°N with highest value of 120

mm/month close to the northeastern Bay (Fig.4.5.3d). In the south the net precipitation showed an increasing trend with maximum value of 180 mm/month near equator.

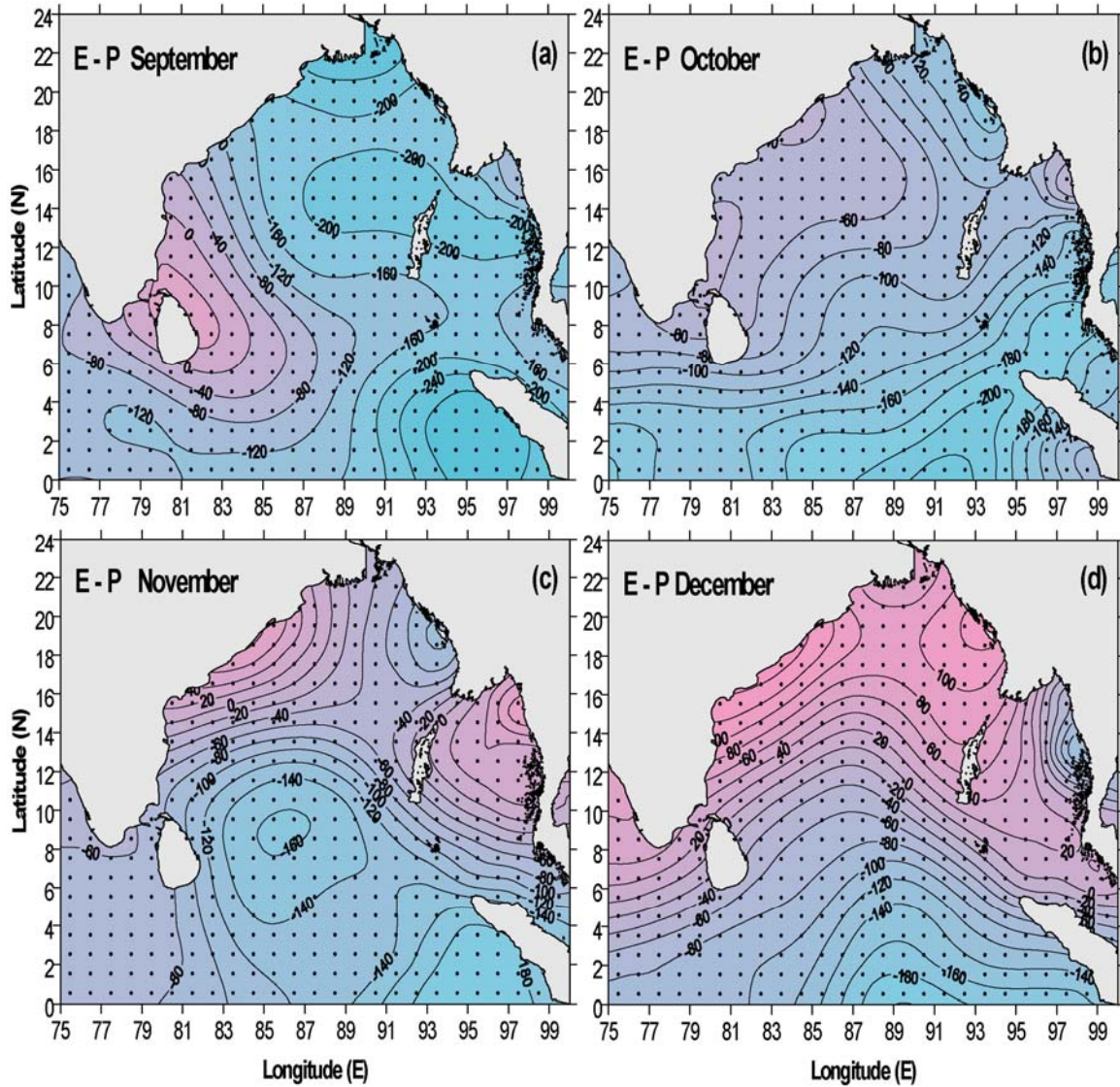


Fig.4.5.3 Monthly mean distribution of E-P (mm/month) in the Bay of Bengal during September to December.

Thus, the amplitude of the seasonal cycle of E-P within the basin was from -440 mm/month to 120 mm/month. The lowest evaporation was about 40 mm/month, which occurred during July-September while highest evaporation was about 120 mm/month

which occurred during December. The lowest precipitation occurred during May, which was about 60 mm/month while highest precipitation was about 440 mm/month which occurred during July. The highest spatial variability occurred during July when E-P varied from 40 mm/month to -440 mm/month. The least spatial variability occurred during May, when E-P varied from 80 mm/month to -60 mm/month. The seasonal cycle of evaporation minus precipitation (E-P) in the northern Bay (north of 15°N) showed annual cycle with positive E-P from December-April and negative E-P during June-September. The seasonal cycle of E-P in the southern Bay (south of 15°N) showed annual variability with net evaporation from February-May and net precipitation from June-December.

4.6 Factors controlling the mixed layer variability

In order to decipher the factors that are responsible for the observed variability in the mixed layer and barrier layer, these were examined in the light of heat flux, momentum flux (wind-stress curl) and fresh water flux (evaporation-precipitation).

4.6.1 Spring intermonsoon

The mixed layer depth during the spring intermonsoon (March-April-May) was the shallowest in the Bay of Bengal compared to the rest of the months, particularly during March and April. It varied between 10 and 25 m except in the southwestern region in March and April and near the western boundary in April (Fig.4.6.1.1a). In May, however, the shallow MLD was confined to the region north of 16°N. Another region of comparatively shallow MLD (~ 25 m) was seen in a band between 6° and 9°N (Fig.4.6.1.1c). The rest of the basin, however, showed deep MLD (30-35 m).

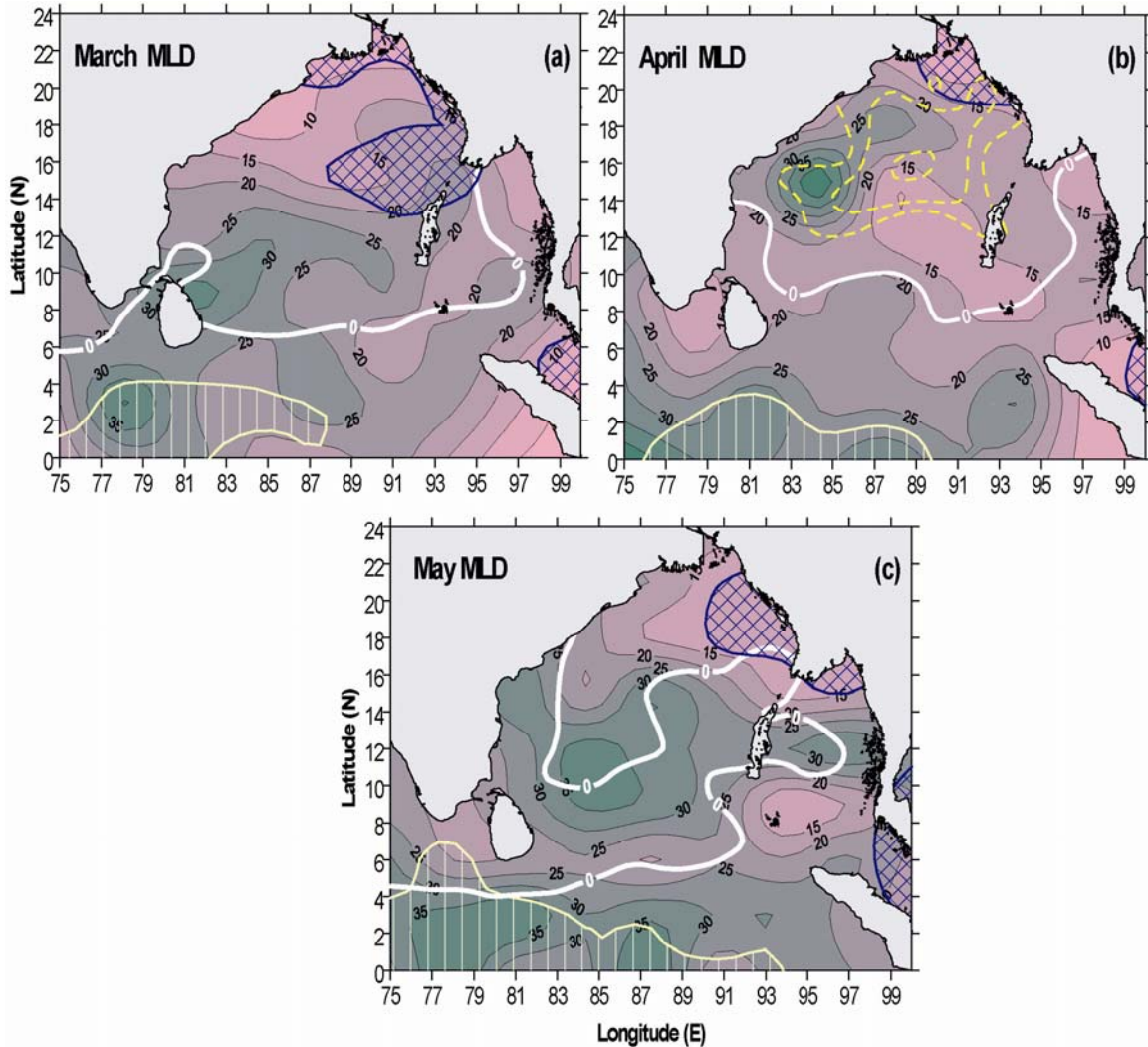


Fig.4.6.1.1 Spatial distribution of mixed layer depth in spring intermonsoon. The blue cross-hatch represents the region where salinity is less than 32 psu while vertical lines within the thin yellow solid line represent the region where the salinity is greater than 34.5 psu. The thick broad white line indicates the zero wind stress curl. The yellow broken lines in (b) indicate the negative wind stress curl (-10 to -20×10^{-8} Pascal/m) with increasing magnitude towards the centre.

The observed MLD variability could be understood in the light of the prevailing ocean-atmospheric conditions. The incoming solar radiation peaked during March-April with a value of $280-290 \text{ W/m}^2$ (Fig.4.1.1) and the net heat flux also was the highest $150-160 \text{ W/m}^2$ (4.2.1). The basin-wide winds were the weakest during this period ($\sim 4 - 5 \text{ m/s}$), except near the western boundary in April where a core of high wind speed was noticed

(Fig.4.3.1) and a strong negative wind stress curl (Fig.4.4.1). The shallow MLD in March-April was driven by the strong stratification induced by peak solar heating and subsequent highest net heat gain by the ocean. Note that the salinity in the northern Bay (north of 18°N) was less than 32.5 psu during March-April (Fig.3.2.1) which makes the waters highly stratified (Fig.4.6.1.2). The weak winds during this period were unable to drive deep wind-mixing due to strong stratification and hence led to the formation of shallow mixed layer.

In the south, the comparatively deeper mixed layer (~ 35 m) seen west of 90°E was due to the presence of high salinity waters (>34.5 psu) which made the water column less stable (Fig.4.6.1.2) and the moderate winds were able to initiate greater mixing leading to the

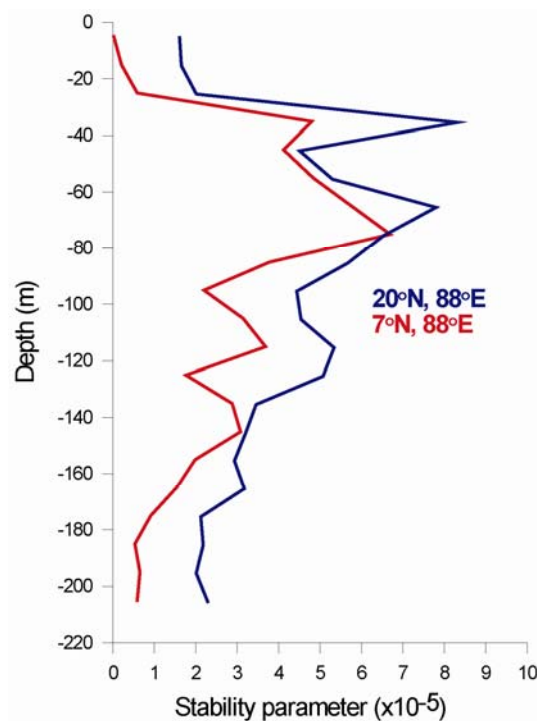


Fig.4.6.1.2 Profiles of upper ocean static stability parameter (E, m^{-1}) at 20°N, 88° E (blue line) and 7°N, 88°E (red line) in the Bay of Bengal during April.

observed deep MLD. However, the deep MLD east of Sri Lanka during March was linked to the development of anti-cyclonic circulation associated with the formation of subtropical gyre which begins in May (Fig.1.2.1). This anti-cyclonic circulation drives down-welling and deepens the mixed layer. The deep MLD along the western boundary (>25 m) in April was driven by the strong negative wind stress curl ($\sim -20 \times 10^{-8}$ Pascal/m, Fig.4.4.1) as could be inferred from the location of the deep MLD and wind stress curl (Fig.4.6.1.1). Note that the subtropical gyre was well developed in April in the central and western Bay of Bengal (Fig.1.2.1), which also leads to down-welling and augments the deepening of the mixed layer. The shallow MLD in the northeastern Bay in May was due to the presence of low salinity waters (~ 32.5 psu, Fig.3.2.2) along with the high incoming solar radiation ($270-280 \text{ W/m}^2$, Fig.4.1.2) which gives rise to strong stratification. The comparatively weaker winds ($5 - 5.5 \text{ m/s}$) in the northeastern region were unable to drive strong wind-mixing and hence the MLD was shallow. Comparatively shallow MLD in a band between 6° and 10°N east of Sri Lanka and southern tip of India was due to the presence of positive wind stress curl in this region (Fig.4.4.2). The deep MLD in the central and western Bay was due to the presence of anti-cyclonic circulation and downwelling associated with the subtropical gyre which occupies the region between western boundary and 90°E (Fig.1.2.1). Again the deep MLD in May in the south, south of 4°N was related to the presence of high salinity waters (>34.5 psu, Fig.3.2.2) and negative wind stress curl (Fig. 4.4.2).

4.6.2 Summer monsoon

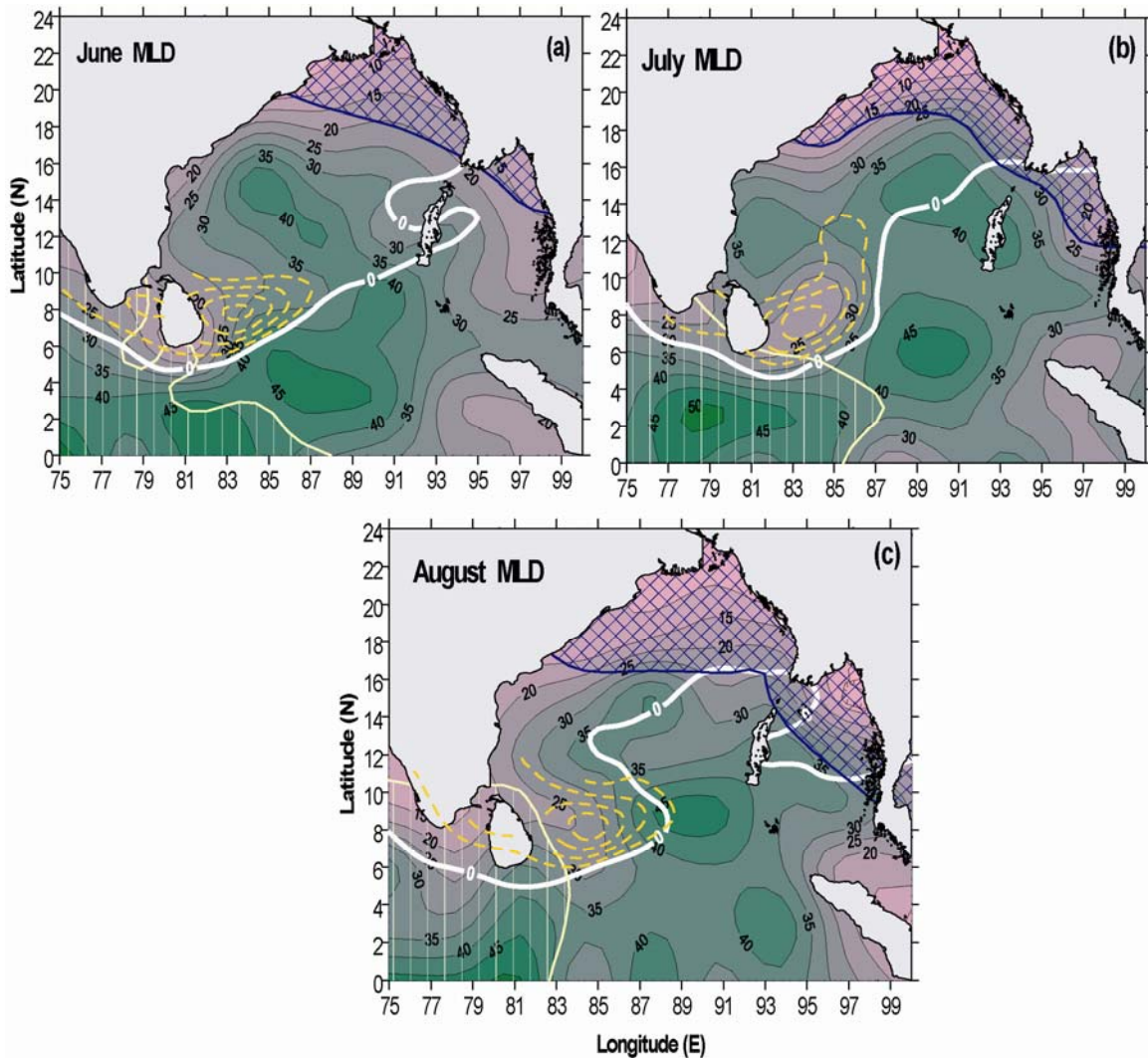


Fig.4.6.2.1 Spatial distribution of mixed layer depth in summer monsoon. The blue cross-hatch represents the region where salinity is less than 32 psu while vertical lines within the thin yellow solid line represent the region where the salinity is greater than 34.5 psu. The thick broad white line indicates the zero wind stress curl. The yellow broken lines in indicate the positive wind stress curl (5 to 20×10^{-8} Pascal/m) with increasing magnitude towards the centre.

Mixed layer during summer monsoon was deep in a band between equator and 6°N (Fig.4.6.2.1), which joined the deep MLD region seen closer to the western boundary towards the end of spring intermonsoon. The northern and eastern part of the Bay had shallow MLD (Fig. 4.6.2.1). With the progress of summer monsoon, the region of deep

MLD expands towards the central and northern Bay. The region around Sri Lanka showed a progressively shallow mixed layer which expanded eastward with time, during summer monsoon. The observed pattern of MLD variation could be explained in the following manner. Though the wind speeds were the highest during summer monsoon in the entire basin (Fig.4.3.2), the MLD were the shallowest in the northern Bay (~ 5m). An examination of E-P showed that it was negative and the highest of all the season, implying excess precipitation, in excess of 440 mm/month, in the northern Bay (Fig.4.5.2). In addition to the oceanic precipitation, the influx of freshwaters from the rivers adjoining the Bay of Bengal also contributed towards freshening of the surface waters of the Bay. An examination of the monthly mean climatology of river discharge of 5 major rivers Ganges, Brahmaputra, Irrawady, Godavari, and Krishna showed that the freshwater discharge dominated during July to October (Fig.4.6.2.2). The spreading of low salinity waters (<32 psu) were seen from the northern Bay towards the south and east (Fig.4.6.2.1) with the progress of summer monsoon. These low salinity waters strongly stratified the upper ocean as could be inferred from the stability parameter (Fig.4.6.2.3). Note that the upper ocean was very warm with SST in excess of 28.5°C (Fig.3.1.2) which also contributed towards strengthening the stratification. Hence, the winds though were the strongest of all the season, it was unable to break the stratification to initiate wind-driven mixing and deepen the mixed layer. The shallow MLD seen around Sri Lanka, irrespective of the low E-P implying excess evaporation (Fig.4.5.2), was driven by the positive wind stress curl (Fig.4.6.2.1). The positive wind stress curl was seen developing in May (Fig.4.4.2) which peaks in June (Fig.4.4.2) and collapses by September (Fig.4.4.3). The positive wind stress curl drives an upward Ekman pumping and this led

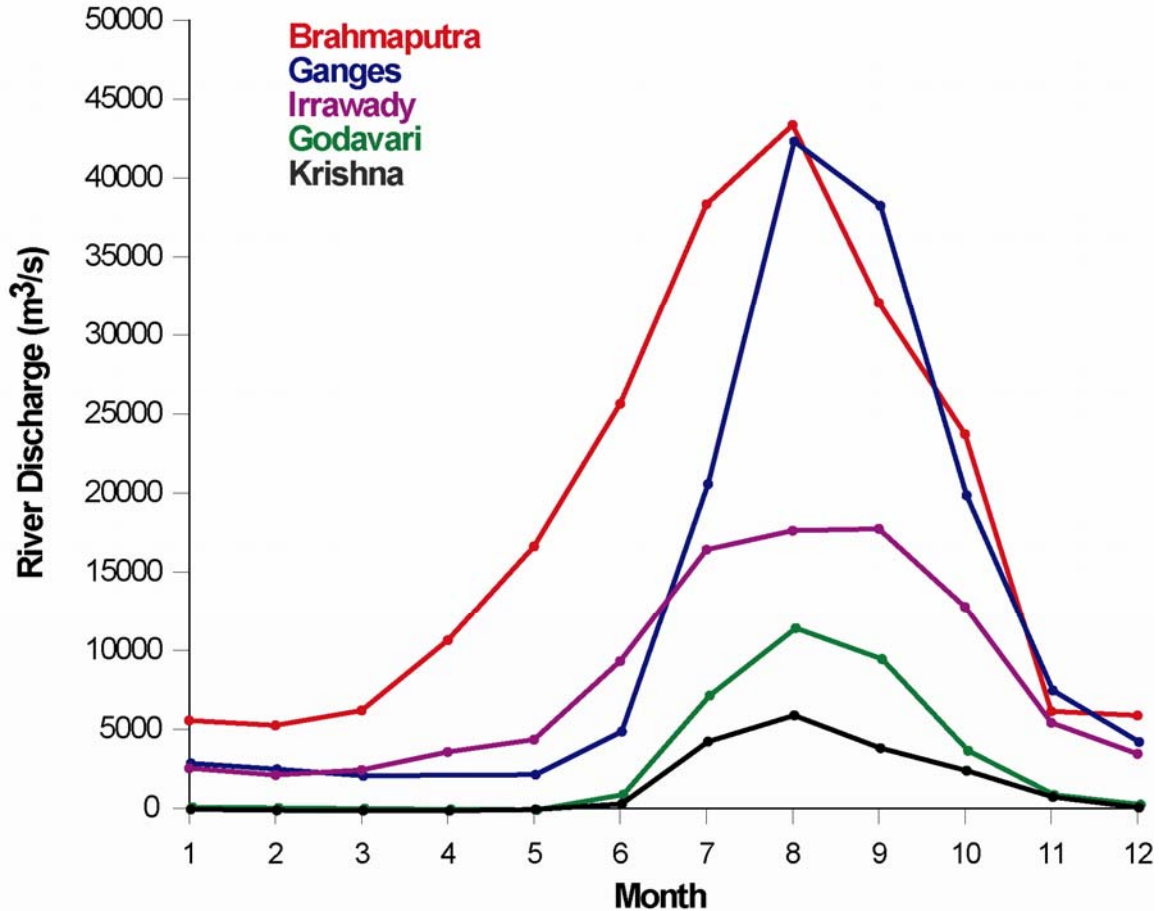


Fig.4.6.2.2 Monthly mean river discharge ($\text{m}^3 \text{s}^{-1}$) climatology of Ganges, Brahmaputra Irrawady, Godavari and Krishna

to the observed shallow mixed layer during summer monsoon. The band of deep mixed layer seen extending from the southwestern region into the central Bay was linked to the advection of high salinity waters from the Arabian Sea. An examination of SSS showed that the high salinity waters from the Arabian Sea was progressively advecting into the central Bay around Sri Lanka during summer monsoon (Fig.3.2.3). This high salinity waters reduced the stratification of the upper ocean as could be inferred from the stability parameter (Fig. 4.6.2.3). Thus, the high winds of the summer monsoon combined with

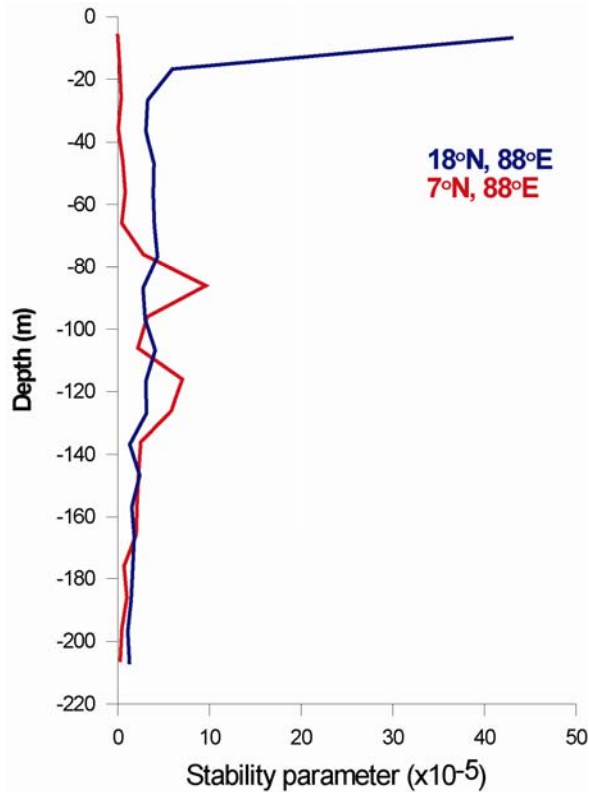


Fig.4.6.2.3 Profiles of upper ocean static stability parameter (E, m^{-1}) at $18^{\circ}N, 88^{\circ}E$ (blue line) and $7^{\circ}N, 88^{\circ}E$ (red line) in the Bay of Bengal during July.

the less stratified upper ocean due to the intrusion of high salinity waters from the Arabian Sea were able to drive strong wind-driven mixing. This was the mechanism which led to the formation of deep MLD in summer. In addition to this, the negative wind stress curl in the central and western Bay also contributed to the observed deep MLD there.

4.6.3 Fall intermonsoon

As the summer monsoon tapers off and the fall intermonsoon sets in, the shallow MLD which was confined to northern Bay, north of $18^{\circ}N$, was seen extending southward to $15^{\circ}N$ in October (Fig.4.6.3.1). This could be explained in the context of changing

atmospheric forcing from summer monsoon to fall intermonsoon. The short wave

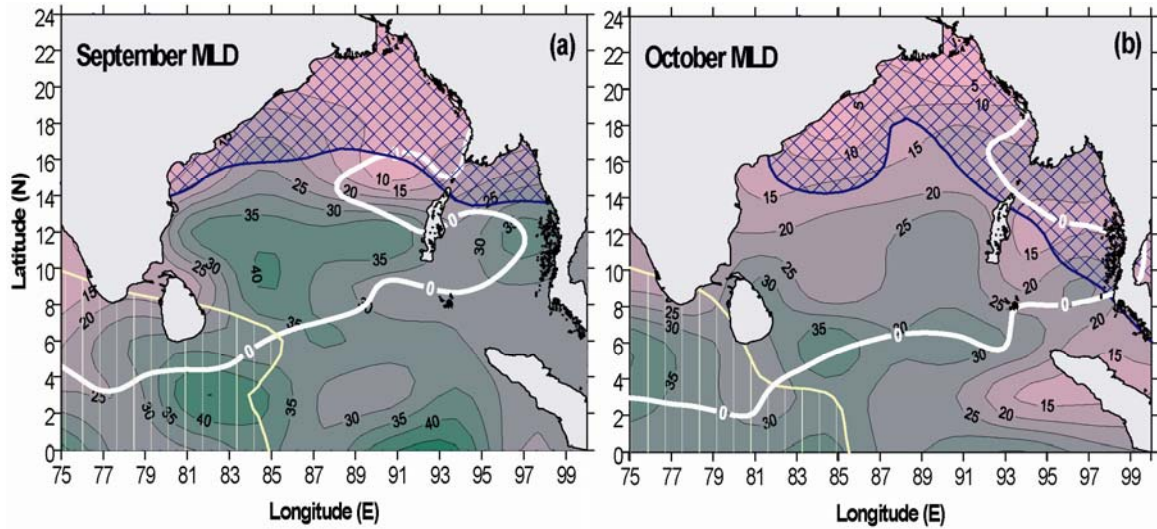


Fig.4.6.3.1 Spatial distribution of mixed layer depth in fall intermonsoon. The blue cross-hatch represents the region where salinity is less than 32 psu while vertical lines within the thin yellow solid line represent the region where the salinity is greater than 34.5 psu. The thick broad white line indicates the zero wind stress curl.

radiation as well as net heat flux showed a secondary heating of the upper ocean during fall intermonsoon (Fig.4.1.3 & Fig.4.2.3) and accordingly the SST was in excess of 29°C in October (Fig. 3.1.3). Though the E-P showed a rapidly decreasing precipitation (Fig.4.5.3), the surface salinity showed a progressive decrease from that of summer monsoon and also a further southward extension of the low salinity waters (Fig.3.2.3). This indicated that the shallow MLD in the northern Bay and its further southward extension was linked to the presence of low salinity waters and its advection southward. As seen from the data, the river discharge was dominant during July to October (4.6.2.2) and hence the low salinity of the surface water was the manifestation of the influence. With the fall intermonsoon the winds over the Bay showed a drastic reduction in their speed in the north (Fig.4.3.3). The high wind speed was confined to the southern Bay. Thus, the deep MLD in the southern Bay was driven by a combination of comparatively

high wind speed and the presence of high salinity waters (Fig.3.2.3) both of which destabilized the water column.

4.6.4 Winter monsoon

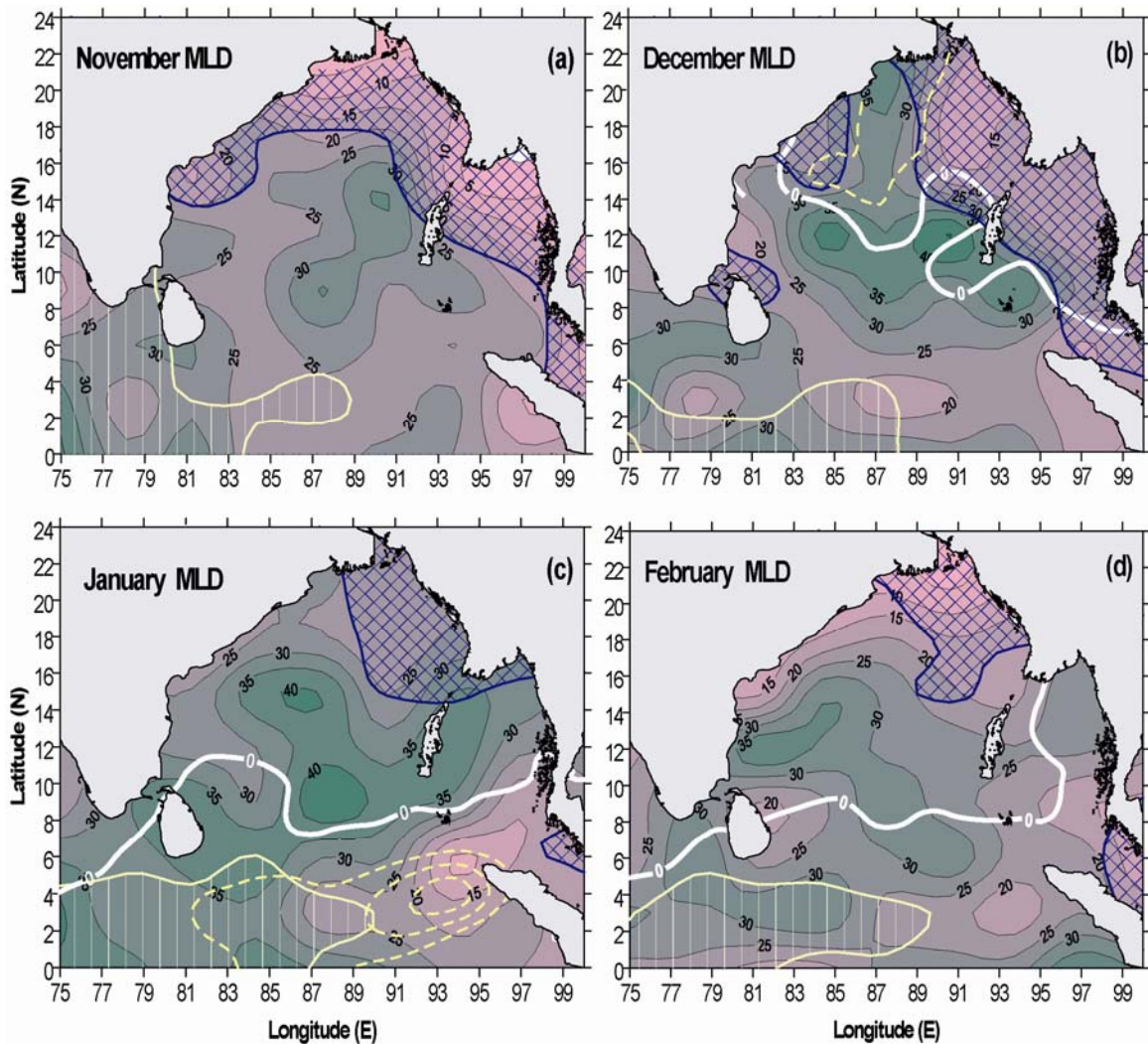


Fig.4.6.4.1 Spatial distribution of mixed layer depth in winter monsoon. The blue cross-hatch represents the region where salinity is less than 32 psu while vertical lines within the thin yellow solid line represent the region where the salinity is greater than 34.5 psu. The thick broad white line indicates the zero wind stress curl. The yellow broken lines in (b) indicate the negative wind stress curl (-5×10^{-8} Pascal/m) while that in (c) indicates the positive wind stress curl (10 to 20×10^{-8} Pascal/m) with increasing magnitude towards the centre.

The winter monsoon in general showed comparatively deep MLD (~30-40 m) all over the Bay except in the north and eastern Bay (Fig.4.6.4.1). The shallow MLD (~5-15 m) in the north and eastern Bay could be explained in the context of the presence of low salinity waters (<32 psu) during November-December (Fig.3.2.3) and associated strong stratification. As the winter progress with E-P showing a net evaporation (Fig.4.5.3) and

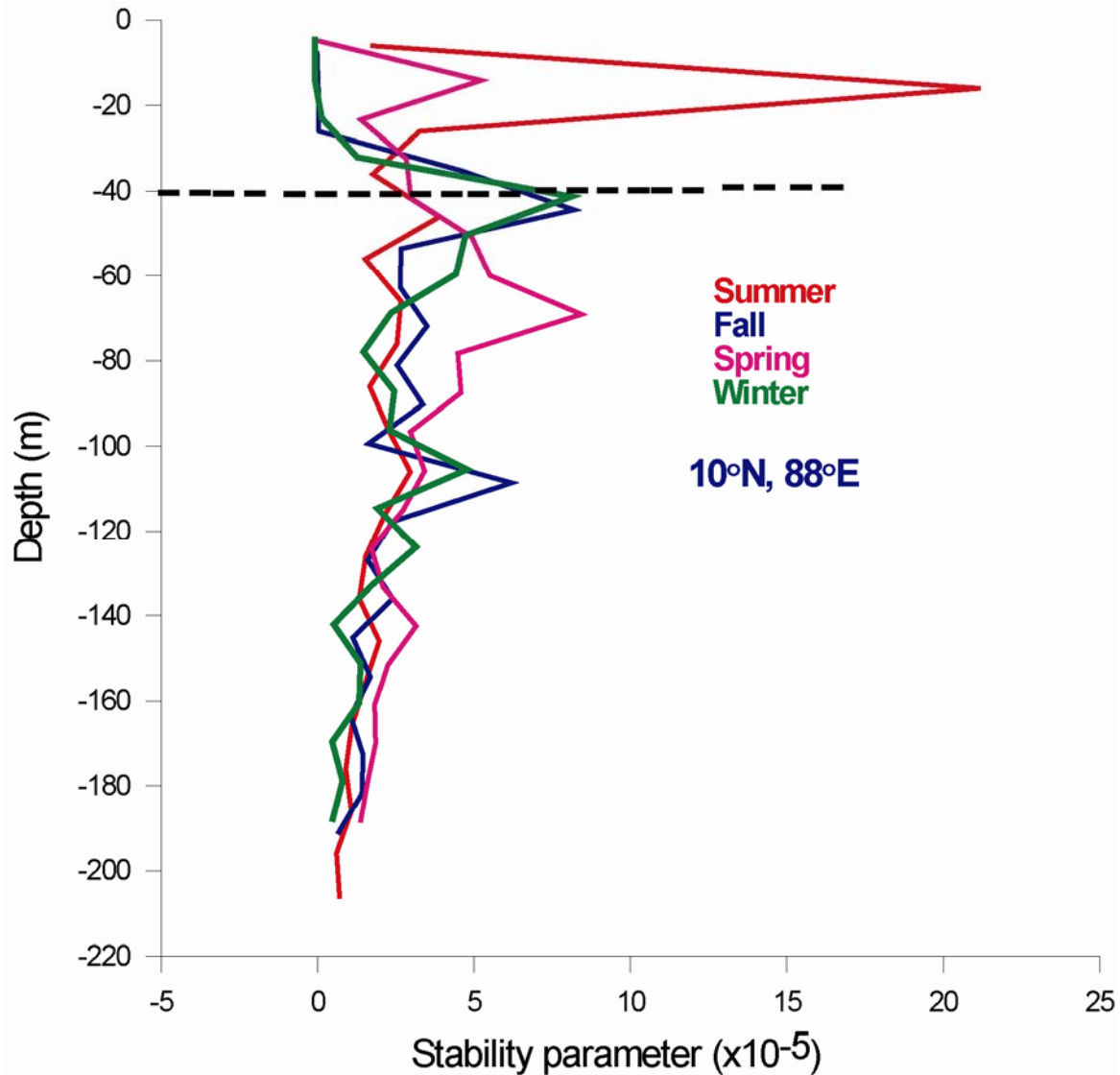


Fig.4.6.4.2 Profiles of upper ocean static stability parameter (E, m^{-1}) at $10^{\circ}N, 88^{\circ}E$ during summer monsoon (red), fall intermonsoon (blue), winter monsoon (green) and spring intermonsoon (pink) in the Bay of Bengal.

retreat to the northern part during January-February (Fig.3.2.1). As a result the area of deeper mixed layer expands further towards eastern boundary. The shallow MLD observed near the Sumatra coast in January was driven by the strengthened positive wind stress curl (Fig.4.4.1) and the associated upward Ekman pumping. The deep MLD in the rest of the Bay was related to the weak stratification that occurred in the Bay during winter monsoon compared to all other seasons, except fall intermonsoon in the upper 40 m (Fig.4.6.4.2). The wind speed, which showed a secondary peak in winter (Fig.4.3.3) were able to initiate deeper wind-mixing as the stratification of the water column was the weakest and this gave rise to the deep mixed layer.

4.6.5 Role of Rossby waves

In order to understand the role of Rossby waves in regulating the MLD the time-longitude plots of sea-level anomaly along latitudes 4° and 16° N were analyzed. For this purpose the sea-level anomaly for the period 1992 to 2006 were used to compute the monthly mean climatology.

The time-longitude plot along 4° N showed bands of alternate positive and negative sea-level anomaly (Fig.4.6.5.1a). These are the signature of westward propagating Rossby waves with positive sea-level anomaly during summer and negative during winter. In summer the central and eastern region showed the highest positive sea-level height anomaly (Fig.4.6.5.1a) and this again contributed to the observed deep MLD in the southern Bay in addition to the reduction in stratification due to the intrusion of high salinity waters from the Arabian Sea.

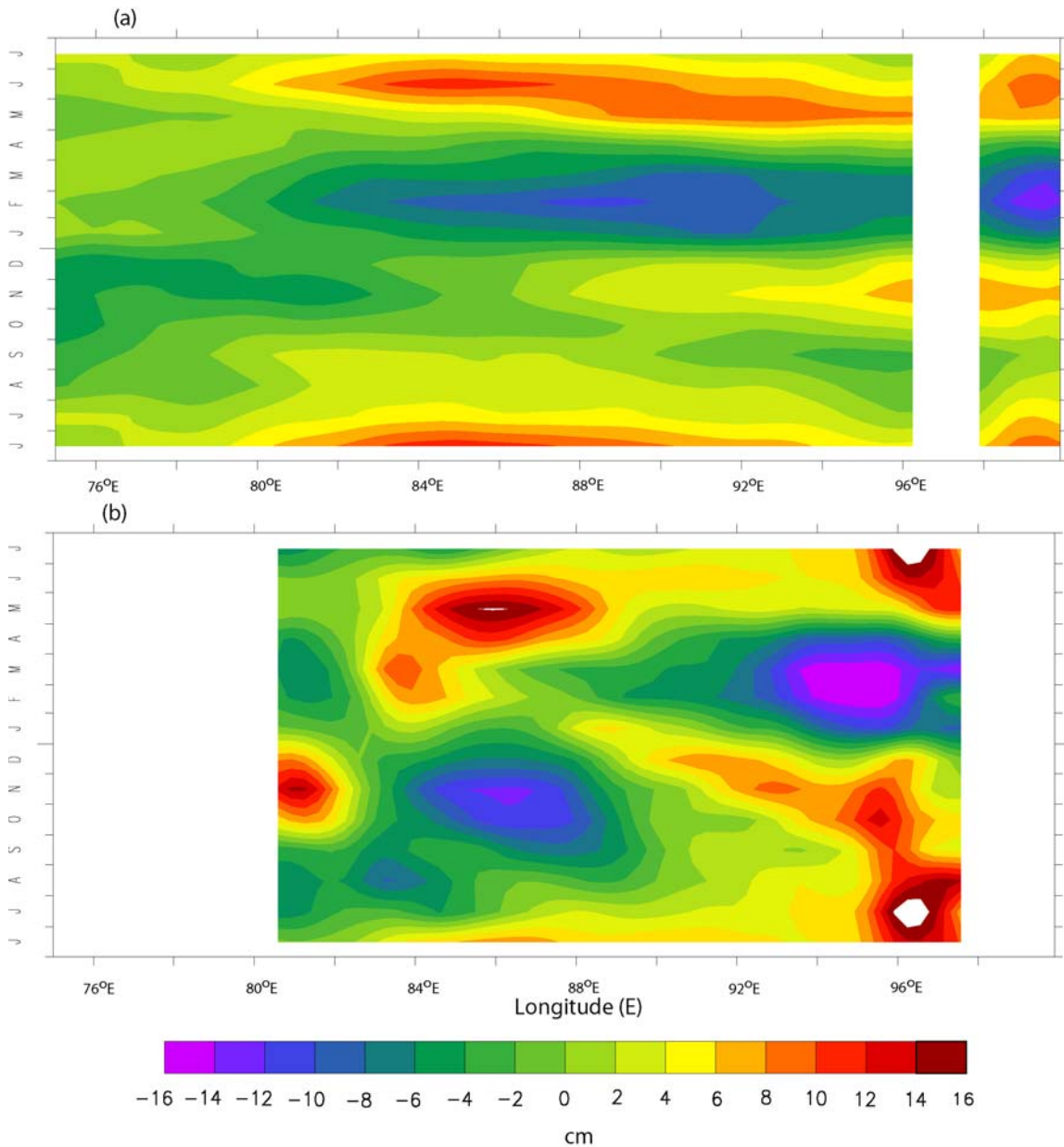


Fig.4.6.5.1 Time-longitude plot of monthly mean sea-level anomaly climatology derived from merged sea-level anomalies of Topex/Poseidon and ERS 1/2 satellites along (a) 4°N and (b) 16°N.

The sloping contours in Fig.4.6.5.1b indicated the signatures of the westward propagating Rossby waves. Close to the eastern boundary the SSH anomaly was negative only during January to April while the rest of the time it was positive. The negative SSH anomaly indicated a shallow MLD, while positive anomaly indicated deep MLD. A patch of

positive SSH anomaly close to the western boundary towards the end of January indicated the development of the western boundary current which peaks in March-April. The region of positive SSH anomaly between western boundary and 90°E was associated with the subtropical gyre, which was the region of deep MLD.

4.7 Factors controlling the barrier layer thickness

The seasonal variability in the barrier layer thickness (BLT) was examined in the context of fresh water flux (E-P) and sea surface salinity (SSS) variability in order to decipher the factors that are responsible for the observed variability.

4.7.1 Spring intermonsoon

The basin-wide barrier layer (BL) thickness was the least in spring intermonsoon (March-April-May) compared to the rest of the seasons (Fig.4.7.1.1). This is due to the lack of freshwater from the river discharge as well as the precipitation during this season. As the occurrence of BL is closely linked to the freshwater flux and salinity distribution, the spatial variation of the barrier layer in the Bay could be understood in the context of freshwater flux, salinity distribution, wind stress curl and prevailing circulation. In March the comparatively thick BL in the northwestern Bay was seen within the region of negative wind stress curl (Fig.4.4.1). In addition, the northern part of the BL was within the low salinity region (<32.5 psu). During March the subtropical gyre with cyclonic circulation develops in the western and central Bay. The observed thick BL was driven by the negative wind stress curl and the prevailing cyclonic circulation. In May the co-location of thick BL in the equatorial regions with that of stronger negative wind stress

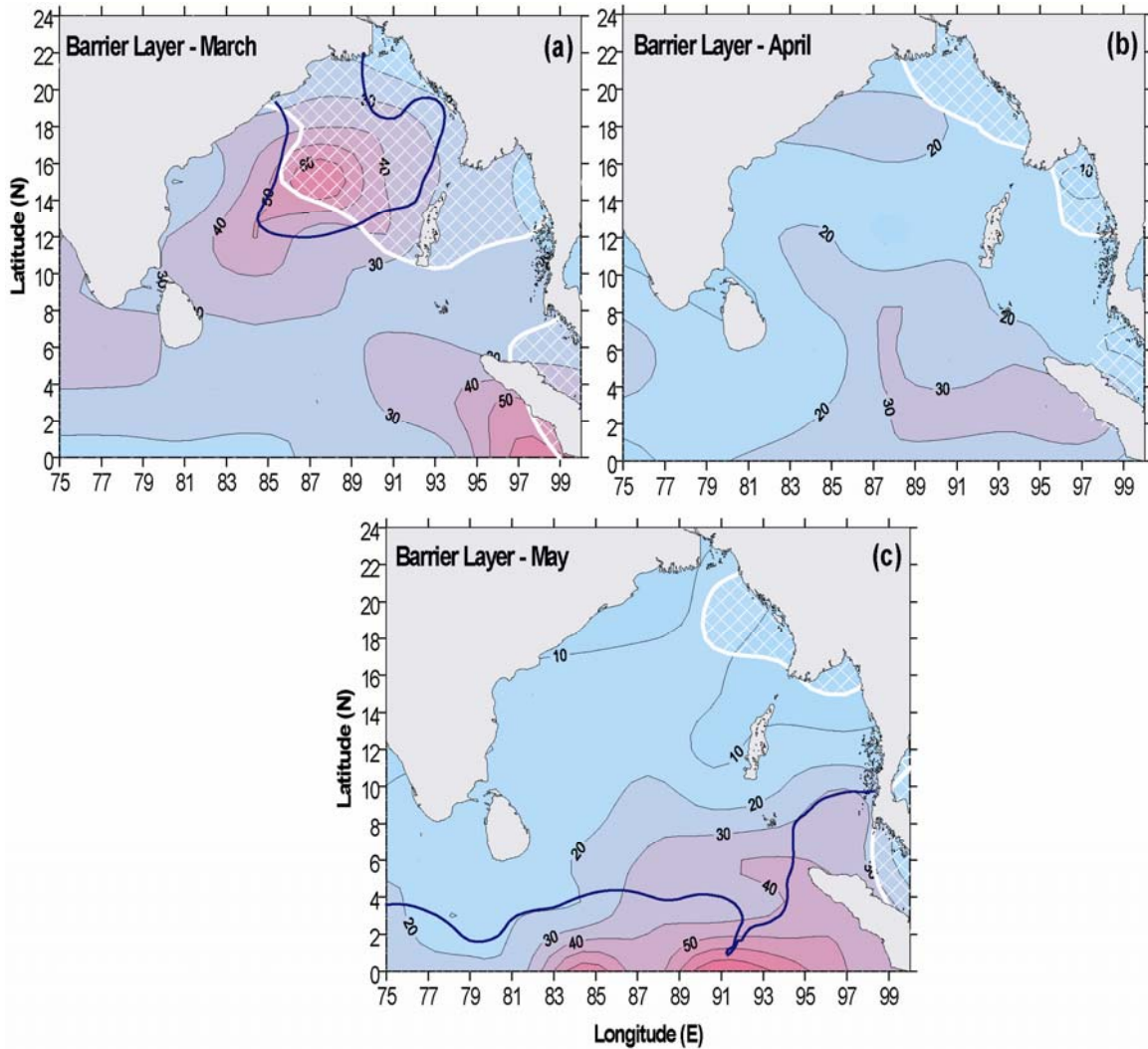


Fig.4.7.1.1 Barrier layer thickness overlaid with salinity less than 32.5 psu (white cross hatch) and negative wind stress curl (5×10^{-8} Pascal/m, solid blue line) during spring intermonsoon.

curl ($5-10 \times 10^{-8}$ Pascal/m) implied the role of wind. Thus, the basin-wide thin BL thickness in the spring intermonsoon was controlled by the strong stratification due to the peak heating and the lack of freshwater input either by the river discharge or through precipitation. The comparatively thick BL in the northwestern Bay was linked to the negative wind stress curl and proximity to the low salinity ambient waters, while that

near the equatorial region was controlled by the negative wind stress curl. The spring-time Wyrтки jet during April-May (Fig.1.2.1) also contributes to the deepening of BL.

4.7.2 Summer monsoon

During summer monsoon (June-July-August) thick BL was noticed along the equatorial region and the eastern boundary of the Bay (Fig.4.7.2.1). The thickest BL occurred near

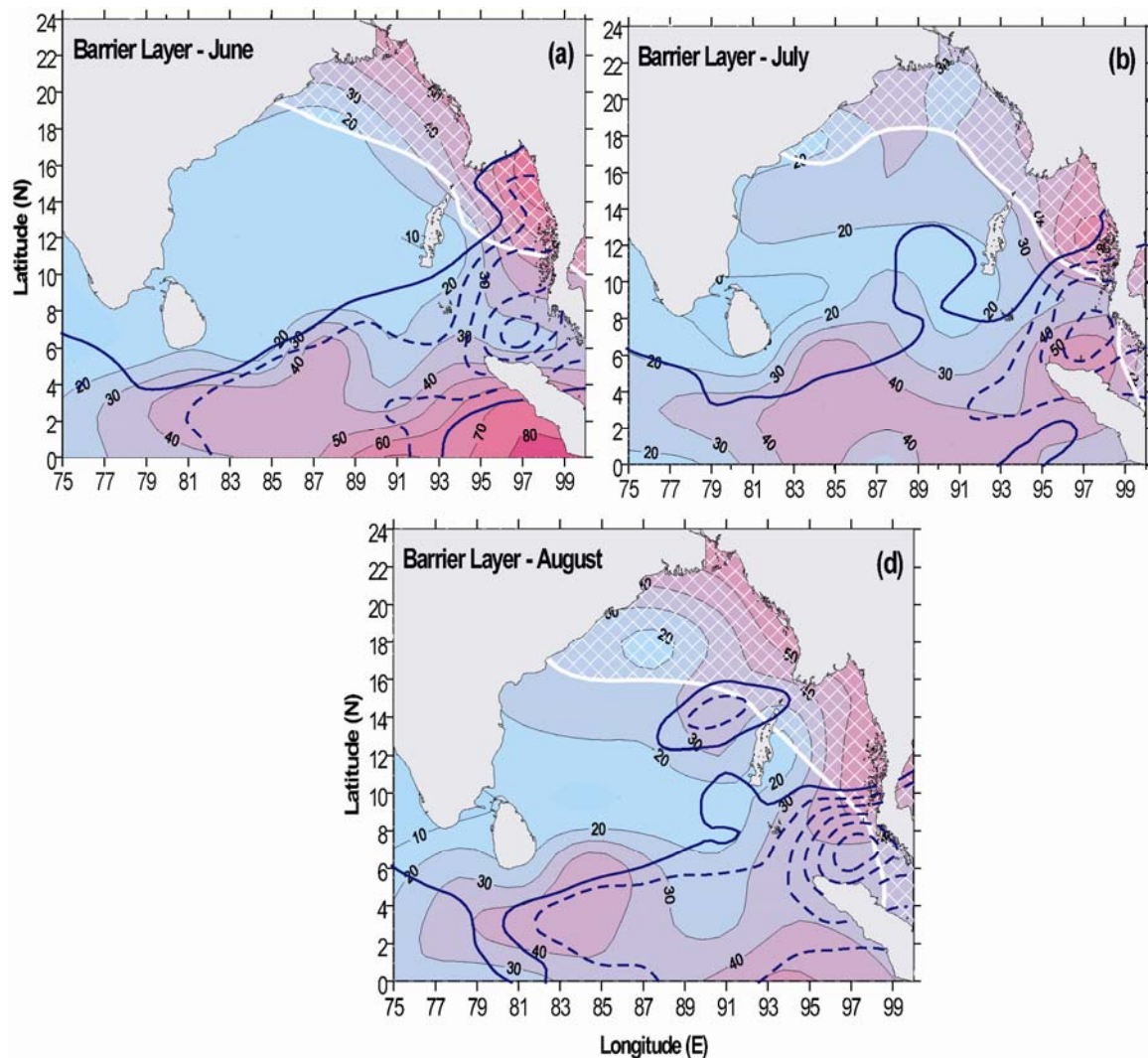


Fig.4.7.2.1 Barrier layer thickness overlaid with salinity less than 32.5 psu (white cross hatch) and negative wind stress curl (solid blue line indicates 5×10^{-8} Pascal/m, and broken blue line indicates values from 10 to 25×10^{-8} Pascal/m) during summer monsoon.

the equatorial region where the negative wind stress curl as well as negative E-P occurred. The negative wind stress curl was the highest in June ($> 20 \times 10^{-8}$ Pascal/m, Fig.4.4.2) near the equatorial region, especially in the eastern region, and showed a decrease in July and August. Accordingly, BL also showed highest thickness in June, followed by July and August. Along the eastern boundary the region of thick BL was located in the region of high precipitation (Fig.4.5.2) and low salinity (Fig.3.2.2) which indicated the role of freshwater flux. In addition, along the southern part of the eastern boundary strong negative wind stress curl occurred. Thus, during summer the thick BL near the equatorial region was driven by wind stress curl, while that along the eastern boundary was due to a combination of large negative wind stress curl as well as the excess precipitation.

4.7.3 Fall intermonsoon

With the tapering of summer monsoon and beginning of fall intermonsoon the BL thickness showed an increase in the eastern equatorial region (Fig.4.7.3.1) which was located within the negative wind stress curl region (Fig.4.4.3). This also was the region of negative fresh water flux (Fig.4.5.3) indicating the contribution of precipitation in the thickness of the BL. In the north, the thick BL was within the region of low salinity (Fig.4.7.3.1). In September the northern Bay in addition to having low salinity also showed excess precipitation. The thick BL in the equatorial region in October was not driven by the negative wind stress curl but by the eastward moving Wyrтки jet (Fig.1.2.1). Note that the fresh water flux was negative in the equatorial region in October (Fig.4.5.3) and the eastward moving Wyrтки jet drives a downwelling.

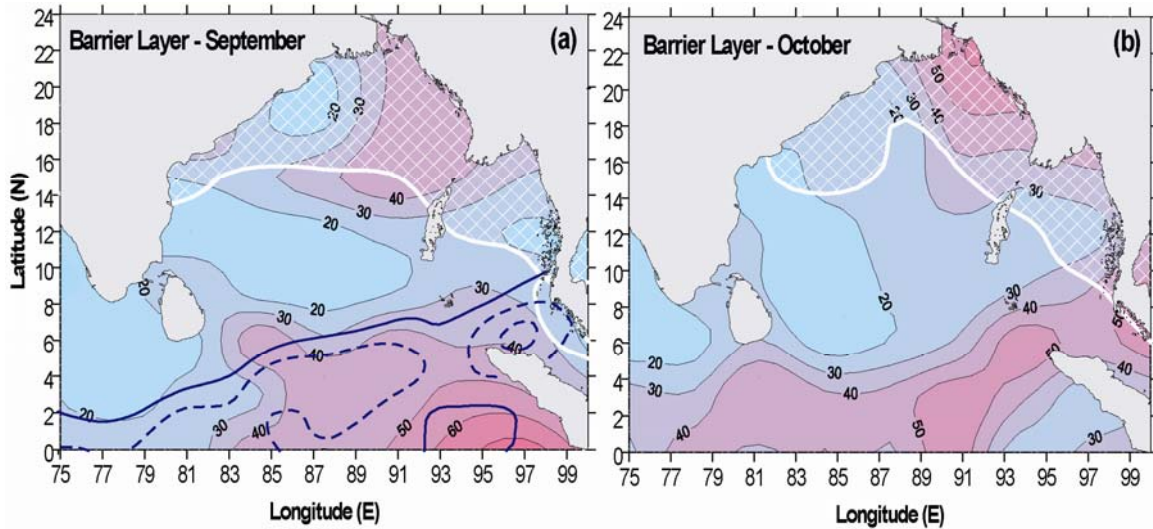


Fig.4.7.3.1 Barrier layer thickness overlaid with salinity less than 32.5 psu (white cross hatch) and negative wind stress curl (solid blue line indicates 5×10^{-8} Pascal/m, and broken blue line indicates values from 10 to 20×10^{-8} Pascal/m) during fall intermonsoon.

4.7.4 Winter monsoon

During winter thick BL was seen along the equator as well as along the eastern and western boundary of the Bay, while the rest of the basin showed comparatively thin BL (Fig.4.7.4.1). Along the equator the BL thickness in November was ~ 40 m which increased during December-January and in February BL thickness reduced considerably in the equatorial region. This could be understood in the context of freshwater flux and prevailing circulation. The fall-time Wyrтки jet flows from west to east was present during November also (Fig.1.2.1). The freshwater flux showed excess precipitation near the equatorial region which peaked during December-January (Fig.4.5.3 & Fig.4.5.1). Thus, the eastward flowing Wyrтки jet will cause down-welling and sinking of surface water which was fresher in winter and gives rise to the observed thick BL along the equatorial region. The thick BL seen in the northeastern and northern region in November

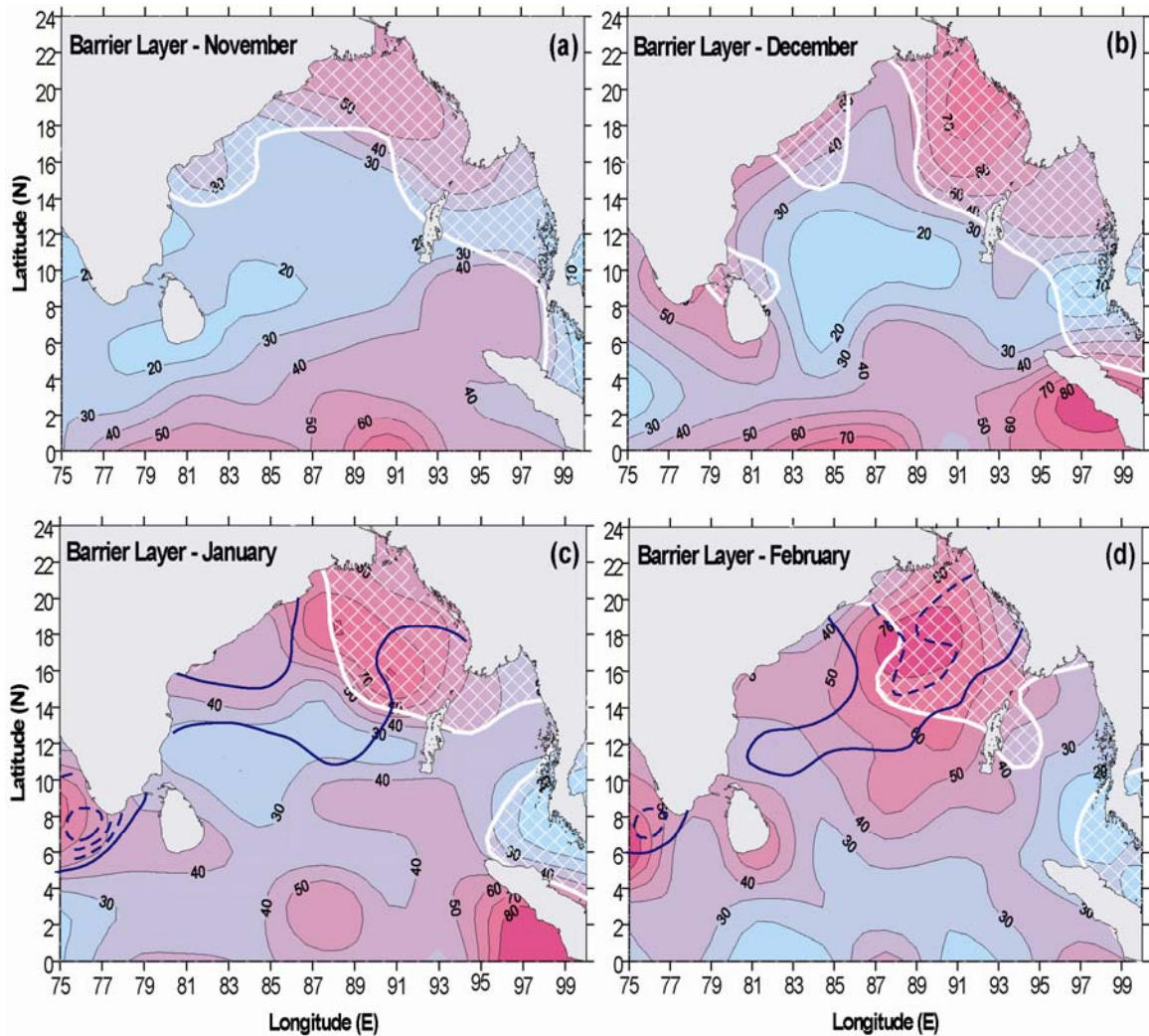


Fig.4.7.4.1 Barrier layer thickness overlaid with salinity less than 32.5 psu (white cross hatch) and negative wind stress curl (solid blue line indicates 5×10^{-8} Pascal/m, and broken blue line indicates values from 10 to 20×10^{-8} Pascal/m) during winter monsoon.

showed a gradual spreading along the western boundary of the Bay during December-January and in February the region of thick BL occupied the northern and central Bay. Note that the region of thick BL occurred within low salinity (< 32.5 psu) region (Fig.4.7.4.1) and the southward spreading of thick BL was associated with the development of East India Coastal Current (EICC). During the mature phase of EICC in December-January it flows southward along the western Bay carrying with it the low

salinity waters from the northern Bay. Thus, the observed spreading of thick BL from the northern-northeastern Bay towards the south along the western boundary and into the west coast of India was driven by the EICC.